

This discussion paper is/has been under review for the journal Atmospheric Measurement Techniques (AMT). Please refer to the corresponding final paper in AMT if available.

A multi-site techniques intercomparison of integrated water vapour observations for climate change analysis

R. Van Malderen¹, H. Brenot², E. Pottiaux³, S. Beirle⁴, C. Hermans²,
M. De Mazière², T. Wagner⁴, H. De Backer¹, and C. Bruyninx³

¹Royal Meteorological Institute of Belgium (RMIB), Uccle, Belgium

²Belgium Institute for Space Aeronomy (BISA), Uccle, Belgium

³Royal Observatory of Belgium (ROB), Uccle, Belgium

⁴Max Planck Institute for Chemistry (MPI-C), Mainz, Germany

Received: 29 November 2013 – Accepted: 22 January 2014 – Published: 6 February 2014

Correspondence to: R. Van Malderen (roeland.vanmalderen@meteo.be)

Published by Copernicus Publications on behalf of the European Geosciences Union.

A multi-site IWV techniques intercomparison

R. Van Malderen et al.

Title Page

Abstract

Introduction

Conclusions

References

Tables

Figures

◀

▶

◀

▶

Back

Close

Full Screen / Esc

Printer-friendly Version

Interactive Discussion



Abstract

Water vapour plays a dominant role in the climate change debate. However, observing water vapour over a climatological time period in a consistent and homogeneous manner is challenging. At one hand, networks of ground-based instruments allowing to retrieve homogeneous Integrated Water Vapour (IWV) datasets are being set up. Typical examples are Global Navigation Satellite System (GNSS) observation networks such as the International GNSS Service (IGS), with continuous GPS (Global Positioning System) observations spanning over the last 15+ yr, and the AERosol RObotic NETWORK (AERONET), providing long-term observations performed with standardized and well-calibrated sun photometers. On the other hand, satellite-based measurements of IWV already have a time span of over 10 yr (e.g. AIRS) or are being merged in order to create long-term time series (e.g. GOME, SCIAMACHY, and GOME-2).

The present study aims at setting up a techniques intercomparison of IWV measurements from satellite devices (in the visible, GOME/SCIAMACHY/GOME-2, and in the thermal infrared, AIRS), in-situ measurements (radiosondes) and ground-based instruments (GPS, sun photometer), to assess the applicability of either dataset for water vapour trends analysis. To this end, we selected 28 sites worldwide at which GPS observations can directly be compared with coincident satellite IWV observations, together with sun photometer and/or radiosonde measurements. We found that the mean biases of the different techniques w.r.t. the GPS estimates vary only between -0.3 to 0.5 mm of IWV, but the small bias is accompanied by large Root Mean Square (RMS) values, especially for the satellite instruments. In particular, we analysed the impact of the presence of clouds on the techniques IWV agreement. Also, the influence of specific issues for each instrument on the intercomparison is investigated, e.g. the distance between the satellite ground pixel centre and the co-located ground-based station, the satellite scan angle, daytime/nighttime differences, etc. Furthermore, we checked if the properties of the IWV scatter plots between these different instruments are dependent on the geography and/or altitude of the station. We could only detect

AMTD

7, 1075–1151, 2014

A multi-site IWV techniques intercomparison

R. Van Malderen et al.

Title Page

Abstract

Introduction

Conclusions

References

Tables

Figures

◀

▶

◀

▶

Back

Close

Full Screen / Esc

Printer-friendly Version

Interactive Discussion



a clear dependency of the RMS, for all considered instruments, on latitude or mean IWV: the RMS of the IWV observations w.r.t. the GPS IWV retrievals decreases with increasing latitude and decreasing mean IWV.

1 Introduction

In climate research, the role of water vapour can hardly be overestimated. First of all, it is the most important natural greenhouse gas as it contributes for about 60 % of the natural greenhouse effect. It also strongly influences atmospheric dynamics and the hydrologic cycle through latent heat transport and diabatic heating, and is, in particular, a source of clouds and precipitation, directly affecting the climate. Unfortunately, clouds are the greatest source of uncertainty in climate models. In a more direct sense, water vapour also provides the largest known feedback mechanism for amplifying climate change (Soden and Held, 2006). Tropospheric water vapour increases in close association with warming, as dictated – under the condition of a constant tropospheric relative humidity – by the Clausius–Clapeyron equation which states that the water holding capacity of the atmosphere goes up at about $7\%K^{-1}$ increase in temperature (Trenberth et al., 2005; Wentz et al., 2007). As a matter of fact, Mears et al. (2007) demonstrated that, on a global scale, both climate models and satellite observations indicate an increase of the total amount of water in the atmosphere over tropical oceans with a rate of $5\text{--}7\%K^{-1}$ of surface warming. Based on data of total column water vapour from measurements with the Global Ozone Monitoring Experiment (GOME) for the period 1996–mid 2003, Wagner et al. (2006) found an increase of about $8\%K^{-1}$ for the tropics, and a comparable or even larger increase for the whole globe ($8\%K^{-1}$ and $12\%K^{-1}$ for the monthly and yearly averages, respectively).

However, finding observational evidence for this relationship over other or smaller regions is complicated by the observational constraints of water vapour: it has a very high temporal and spatial variability, in contrast to other greenhouse gases such as carbon dioxide or methane. For instance, there is a large gradient in the volume mixing

A multi-site IWV techniques intercomparison

R. Van Malderen et al.

Title Page

Abstract

Introduction

Conclusions

References

Tables

Figures



Back

Close

Full Screen / Esc

Printer-friendly Version

Interactive Discussion



A multi-site IWV techniques intercomparison

R. Van Malderen et al.

Title Page

Abstract

Introduction

Conclusions

References

Tables

Figures

◀

▶

◀

▶

Back

Close

Full Screen / Esc

Printer-friendly Version

Interactive Discussion



ratio of water vapour from the ground (approx. 10 000 ppm) to the tropopause (approx. 4 ppm), so that the measurement of tropospheric water vapour is a demanding task (Palm et al., 2010) and explains why there is no standard instrument that will measure it everywhere accurately. Luckily, about 45–65 % of the total column of water vapour is included in the surface-850 hPa layer (Ross and Elliot, 1996). In this paper, we will concentrate on this Integrated Water Vapour (IWV) amount, also commonly known as Precipitable Water Vapour (PW or PWV) or Total Column Water Vapour (TCWV), and we will express the IWV in units of mm. It is defined as the liquid equivalent of the total water vapour contained in an air column from the Earth's surface to the top of the atmosphere (Wang et al., 2007). This primary atmospheric variable can be measured by different devices, among which ground-based, satellite-based and in-situ techniques and instruments. The most commonly used ground-based instruments for water vapour monitoring are Fourier Transform Infrared (FTIR) spectrometers, microwave radiometers, lidars (for “light detection and ranging”), sun photometers and Global Positioning System (GPS) remote sensing (see e.g. Kämpfer, 2013, for an overview of most of these techniques). Recently, Wagner et al. (2013) developed an algorithm for the retrieval of the atmospheric water vapour column from Multi-AXis Differential Optical Absorption Spectroscopy (MAX-DOAS) ground-based observations in the yellow and red spectral range. In-situ measurements by radiosondes have been used regularly since the 40s to measure the water vapour in the atmosphere and have widely been used to determine IWV trends in the literature (e.g. Ross and Elliott, 2001; Durre et al., 2009; Mattar et al., 2011). On meteorological satellites, the total precipitable water vapour is sounded using visible, near infrared, thermal infrared, passive microwave, and radio-occultation techniques (Urban, 2013). It should be clear that each of these techniques has their strengths and weaknesses, and need to be inter-compared carefully under different conditions if progress is to be made on understanding the water vapour distribution and its time variability. However, Buehler et al. (2012) concluded that a literature survey reveals that reported systematic differences between different techniques are study-dependent and show no overall consistent pattern. Further

improving the absolute accuracy of IWV measurements and providing climate-quality time series therefore remain challenging problems.

The present study aims (1) to evaluate the quality and the consistency between different techniques measuring the IWV and (2) to assess the applicability of either datasets for water vapour time series analysis and climate trend detection. Although an IWV techniques intercomparison has been the subject of at least a dozen of papers in the literature (see Buehler et al., 2012, for a number of these, and Hocke and Martine, 2013, for tables of intercomparison studies), the added value of our analysis lies in focusing on homogeneous datasets or datasets taking part in a homogenisation procedure. Moreover, several studies in the literature concentrate on a multi-sensor intercomparison at a single site (e.g. Palm et al., 2010; Schneider et al., 2010; Buehler et al., 2012). In this paper, we will first focus on the mid-latitude site Brussels (Belgium), as a case study (see Sect. 4), but subsequently extend our analysis to a set of 28 stations world-wide, to investigate the geographical dependency of the differences between the IWV datasets generated from different techniques. As an at least partly cloud free sky is needed for water vapour observations by numerous techniques, a secondary aim of our study is therefore to study the impact of such an “observation bias” on the IWV differences between different instrumental datasets (this paper) and on the resulting IWV trends (paper in preparation). Finally, based on the literature, we identified for each instrument some specific instrumental issues regarding the IWV retrieval, as e.g. daytime/nighttime differences, sensor type change, (limiting) distance and/or height difference for co-location, satellite scan angle. A last goal of this paper is to investigate the influence of these different issues on the agreement between IWV values retrieved by different techniques.

The paper is organised as follows. In Sect. 2, we discuss the different instruments and datasets used for monitoring the water vapour. A special emphasis is given on the (reported) uncertainties of the IWV retrieval for each technique. The general methodology used for the techniques intercomparison is covered in Sect. 3. This methodology is then applied to the station at Brussels, Belgium, in Sect. 4, and to our world-wide

A multi-site IWV techniques intercomparison

R. Van Malderen et al.

Title Page

Abstract

Introduction

Conclusions

References

Tables

Figures



Back

Close

Full Screen / Esc

Printer-friendly Version

Interactive Discussion



selection of 28 stations in Sect. 5. The last section, Sect. 6, is reserved for drawing the conclusions and discusses the outlook.

2 Instruments and datasets

The IWV can be obtained using a large variety of techniques and instruments from which a selection was made and presented in this paper. This selection is far from being complete, but we included devices that were identified as promising for studying IWV trends for climate change analysis, based on the length of their time series and their data quality and homogeneity. This study focuses over land as we want to include some promising ground-based devices. Consequently we are omitting microwave satellite IWV measurements over ocean, often used as reference for global trend analysis and climate model intercomparisons, and playing a prominent role in the EUMETSAT Operational climate monitoring from space initiative that will blend different satellite instruments. A techniques intercomparison study over ocean including these microwave measurements has already been described in Mieruch et al., 2010.

In this section, we describe how IWV values are derived for each technique and instrument, their reported accuracies, their susceptibility to a weather bias (or not) and the main characteristics of the corresponding IWV databases (length, coverage, homogeneity, etc.). A summary of these characteristics is given in Table 1.

2.1 GPS

Since 1997, the IGS (International GNSS Service, Dow et al., 2009) has provided the scientific community operationally with high-precision tropospheric Zenith Total Delay (ZTD) estimates based on GPS observations recorded by continuously operating stations of its global network. Using surface measurements of pressure and temperature, these ZTD values can be turned into IWV values (Bevis et al., 1992; Rocken et al., 1995; Ware et al.; 1997) and used for atmospheric research.

A multi-site IWV techniques intercomparison

R. Van Malderen et al.

Title Page

Abstract

Introduction

Conclusions

References

Tables

Figures



Back

Close

Full Screen / Esc

Printer-friendly Version

Interactive Discussion



A multi-site IWV techniques intercomparison

R. Van Malderen et al.

Title Page

Abstract

Introduction

Conclusions

References

Tables

Figures



Back

Close

Full Screen / Esc

Printer-friendly Version

Interactive Discussion



However, the methodology used by the IGS to produce these ZTDs (i.e. the IGS final troposphere product) has evolved along the time, leading to inconsistencies in the derived IWV time series. To solve this problem, the IGS started a back-processing of all historical GPS data using a single uniform strategy to insure the consistency and homogeneity of its tropospheric product time series (i.e. ZTDs and North and East gradient components every 5 min). Thanks to the length of its time series (15+ yr) and the world-wide location of the IGS stations, one scientific value of the reprocessed IGS troposphere product is clearly climatology.

The public release of the reprocessed IGS troposphere products was announced in November 2011 (Byun and Bar-Sever, 2010). The products are based on GPS-only observations and were computed with the GIPSY software using the Precise Point Positioning (PPP) technique (Zumberge et al., 1997). Details on the reprocessing analysis strategy are provided in Byun and Bar-Sever (2009). The reprocessing was applied to the complete IGS network i.e. about 400 continuously operating GPS stations (Dow et al., 2009), from 1995 until end 2007. This reprocessing is fully consistent with the strategy used by the IGS to produce the operational IGS final troposphere products from 2008 to April 2011 and provides thus access to 15+ yr of continuous, world-wide and spatially well distributed IWV values. After this date, the IGS orbit and clock products are based on the new IGS08 terrestrial reference frame (Rebischung et al., 2012) and the new igs08.atx antenna models (Schmid, 2011) and the consistency is not guaranteed anymore (Ray, 2011). This problem will be overcome when the next IGS backprocessing will take place¹.

2.1.1 ZTD to IWV conversion scheme

The ZTD computed from raw GPS data represents the total delay induced by the neutral atmosphere on the GPS signal propagation in the zenith direction. It includes the

¹In the remaining of the text we will use “IGS troposphere product” for the IGS reprocessed tropospheric products (1995–2007) or the IGS final tropospheric product (2008–April 2011).

A multi-site IWV techniques intercomparison

R. Van Malderen et al.

Title Page

Abstract

Introduction

Conclusions

References

Tables

Figures

◀

▶

◀

▶

Back

Close

Full Screen / Esc

Printer-friendly Version

Interactive Discussion



delay due to whole the density of the neutral atmosphere (named the Zenith Hydrostatic Delay, ZHD) and an additional delay induced by the water vapour (called the Zenith Wet Delay, ZWD). To be used in climate applications, ZTDs are usually converted to IWVs to remove the hydrostatic effect and keep only the effect of the influence of the water vapour. Therefore, the ZWD is first obtained by subtracting the ZHD from the ZTD (all in m),

$$\text{ZWD} = \text{ZTD} - \text{ZHD} \quad (1)$$

Assuming the hydrostatic equilibrium of the neutral atmosphere, the ZHD at a given GPS station can be modelled using the surface pressure (P_s in hPa) and an estimation of the gravity (g_m) of the centre of the atmospheric column (Saastamoinen, 1972; Davis et al., 1985; Elgered et al., 1991), where g_m depends on the latitude ϕ (in degrees) and the height h of the station above the Earth ellipsoid (in m):

$$\text{ZHD} = (0.0022768 \pm 5 \cdot 10^{-7}) \cdot P_s / (1 - 0.00266 \cos 2\phi - 0.000000279 \cdot h) \quad (2)$$

In a second step, the IWV (in kgm^{-2} or mm) is retrieved from the ZWD using the following relationship (Hogg et al., 1981; Askne and Nordius, 1987; Bevis et al., 1992):

$$\text{IWV} = \kappa(T_m) \cdot \text{ZWD}, \quad (3)$$

with $\kappa(T_m)$ a proportionality factor containing constants like the specific gas constant of water vapour, the density of liquid water, atmospheric refraction constants and varying with the water vapour weighted mean temperature of the atmosphere T_m (Bevis et al., 1992). T_m can be either calculated from vertical profile data provided by the global re-analyses of the European Centre for Medium-Range Weather Forecasts (ECMWF) and the National Centers for Environmental Prediction (NCEP) or estimated from surface temperature (T_s) observations using a linear empirical relationship (e.g. Bevis et al., 1992), the so-called $T_m - T_s$ relationship:

$$T_m = 70.2 + 0.72 \cdot T_s \quad (4)$$

A multi-site IWV techniques intercomparison

R. Van Malderen et al.

[Title Page](#)[Abstract](#)[Introduction](#)[Conclusions](#)[References](#)[Tables](#)[Figures](#)[Back](#)[Close](#)[Full Screen / Esc](#)[Printer-friendly Version](#)[Interactive Discussion](#)

According to Wang et al. (2005), the estimation of T_m using this latter relationship underestimates T_m in the tropics and subtropics by up to 6 K and overestimates T_m in the mid and high latitudes by up to 5 K. In a forthcoming paper, we will go more into detail in those differences in T_m and the impact on the derived IWV. For our techniques intercomparison, we chose to calculate T_m from the surface temperature observations, because we aim at an IWV intercomparison analysis on a purely observational basis without the mixing of model output data with observations. Furthermore, the time resolution of the global reanalyses is at maximum 6 h, so that an interpolation of the model output would be necessary to create GPS-based IWV values that coincide within a smaller time interval with measurements from another device. This is feasible, but does not fit completely within the purely observational techniques intercomparison we want to present in this paper.

To conclude, we need coincident surface pressure and temperature measurements at an IGS station to convert the ZTDs to IWV values. Unfortunately, only a minority of the IGS stations are equipped with pressure and temperature sensors (about 70 IGS sites were equipped with pressure sensors in 2009, see Vey et al., 2009). Moreover, these sensors are not necessarily regularly calibrated. Therefore, we will rely on the surface pressure and temperature observations from the large database of the World Meteorological Organization (WMO). These data were accessed via the Global Telecommunication System (GTS) or via the ECMWF. The maximum separation distance between the IGS and the WMO stations was restricted to 50 km and the height difference is taken into account by adjusting the surface values from the synoptic station height to that at the IGS station height: for the surface temperature adjustment, we assume a standard lapse rate of -6.5 K km^{-1} , typical for wet adiabatic conditions, and the hydrostatic and ideal gas equations are used to adjust the surface pressure. Hagemann et al. (2003) and Vey et al. (2009) showed that the pressure observations from neighbouring WMO stations represent very well the pressure at the GPS stations, provided that the synoptic station is located within 50 km of the GPS site and that the altitude differences between the two locations is less than 100 m (Gutman et al., 2003).

We will come back to this point in Sect. 3.2. We also stress that we do not perform any temporal interpolation of the surface measurements, but use them at their actual observation times.

2.1.2 Uncertainty of the GPS-based IWV

To estimate the uncertainty of GPS-based IWVs three error sources have to be considered: (1) the uncertainty of the ZTD estimations, (2) the uncertainty of the ZHD modelling (Eq. 2), and (3) the uncertainty of the conversion from ZWD to IWV (Eqs. 3 and 4). Of these three, the main error source are the ZTD uncertainties, due to modelling limitations in the GPS analysis.

As an indicator of the uncertainties of the ZTD estimates, we analysed the formal error of the reprocessed IGS troposphere product over the complete set of IGS stations and over the whole period (1995–April 2011). The result of this analysis is illustrated in Fig. 1. This histogram shows that the formal ZTD error ranges from 0.8 to 10 mm. 95 % of the ZTDs have a formal error below 2.6 mm and 99.9 % of them have a formal error below 4.4 mm. This is somewhat better than the finding of Byun and Bar-Sever (2009), which analysed a subset of 30 globally distributed IGS stations during 2003 and found a formal error between 1.5 and 5 mm of ZTD. Of course, this formal error does not take into account systematic errors (e.g. in GPS orbits and clocks) and is therefore slightly underestimating the actual error. With a claimed accuracy of the IGS ZTD product of 4 mm, Deblonde et al. (2005) derived a corresponding error of 0.6 mm in IWV.

The ZHD is basically obtained from the surface pressure based on the hydrostatic equilibrium hypothesis (see Eq. 2), and the accuracy of the ZHD modelling is therefore mainly dependent on errors in the air pressure measurement, causing offsets in the IWV estimates of at most 0.8 mm when considering an error in the pressure of 2 hPa (Vey et al., 2010). Other surface pressure estimates reported in the literature are 1 hPa (Deblonde et al., 2005) and 1.65 hPa (Wang et al., 2007), corresponding respectively to 0.4 and 0.6 mm uncertainty in IWV. Only during extreme (and rare) events, the

A multi-site IWV techniques intercomparison

R. Van Malderen et al.

Title Page

Abstract

Introduction

Conclusions

References

Tables

Figures



Back

Close

Full Screen / Esc

Printer-friendly Version

Interactive Discussion



atmosphere departs from hydrostatic equilibrium and consequently, this assumption can lead to significant errors in the IWV estimation (Brenot et al., 2006).

Finally, the last source of uncertainty comes from the estimation of the proportionality factor $\kappa(T_m)$ in Eq. (3), which depends primarily on the mean atmospheric temperature.

When calculated from the surface temperature as in Eq. (4), the uncertainty in the mean atmospheric temperature is estimated to be around 5 K (or 1.8 % for $T_m = 273$ K), which corresponds to an IWV error of 0.07 mm to 0.72 mm for resp. a dry or moist atmosphere (Deblonde et al., 2005). The corresponding mean IWV error of 0.3 mm reported by Brenot et al. (2006) lies in this range.

When summing up these three error sources, the final uncertainty of GPS-based IWV measurements is generally less than 2 mm. These estimations agree with previous studies of other authors where uncertainties are obtained by comparison with water vapour radiometers and radiosondes (Kuo et al., 1993; Rocken et al., 1993, 1995; Businger et al., 1996; Duan et al., 1996; Tregoning et al., 1998).

2.2 CIMEL sun photometer

A CIMEL sun photometer measures the sun and sky transmittance at selected wavelengths (filters) centred between 340 and 1020 or 1640 nm in an automated mode. Its field-of-view is 1.2° . Direct sun measurements are typically performed every 15 min between sunrise and sunset, under clear sky condition. A CIMEL sun photometer is able to retrieve the IWV and the aerosols properties (e.g. the aerosol optical depth, Ångström exponent, single scattering albedo) using a combination of spectral filters and azimuth/zenith viewing controlled by a microprocessor. Using the 940 nm channel, centred on the 946 nm water vapour absorption line, the water vapour transmittance can be determined after first accounting for aerosol effects (using the 675 and 870 nm channels). Using a power law parameterisation, a conversion of the slant optical depth to the slant IWV can be obtained (e.g., Bruegge et al., 1992; Schmid et al., 2001). Uncertainties in this parameterization and the Langley plot regression (due to variable atmospheric water vapour amounts) as well as deficits in the filter characterisation are

A multi-site IWV techniques intercomparison

R. Van Malderen et al.

Title Page

Abstract

Introduction

Conclusions

References

Tables

Figures



Back

Close

Full Screen / Esc

Printer-friendly Version

Interactive Discussion



the leading error sources. Alexandrov et al. (2009) estimate an IWV precision of about 10% for this technique.

The CIMEL instrument is the standard instrument used in the AERONET (AERosol RObotic NETwork) international network (<http://aeronet.gsfc.nasa.gov>). AERONET provides a long-term, continuous and readily accessible public domain database of aerosol optical, microphysical and radiative properties for aerosol research and characterization, validation of satellite retrievals, and synergism with other databases. The network is currently dense in Europe and the Americas. The data used in this paper is processed and archived with the version 2 of the AERONET IWV retrieval algorithm, defined as the quality-assured level (Holben et al., 2006). All the instruments in the AERONET are more or less annually calibrated with the Mauna Loa Observatory as the world standard reference.

The IWV retrieval with this instrument is limited to daytime and clear skies. This introduces a negative fair weather bias in the recorded IWVs, since cloudy conditions are often associated with higher IWV values. The reported IWV value in the AERONET database is the zenith value, but the solar slant value can easily be found back using the optical air mass table based on a standard atmosphere (Kasten and Young, 1989).

2.3 Radiosondes

Radiosondes (RS), launched on weather balloons since decades throughout the world, provide vertical profiles of pressure, temperature, relative humidity (or dew point temperature), wind speed and wind direction. The primary source of radiosonde data used in this paper was the Integrated Global Radiosonde Archive (IGRA, Durre et al., 2006). The IWV can be calculated from the IGRA sounding data if the required observations of pressure, temperature, and dew point depression are available at the surface and all mandatory above-surface levels up to and including 500 hPa. The calculation involves the conversion of dew point depression to specific humidity at each suitable significant and mandatory level followed by the integration of specific humidity over all available levels between the surface and 500 hPa (Durre et al., 2009). The upper limit of 500 hPa

A multi-site IWV techniques intercomparison

R. Van Malderen et al.

Title Page

Abstract

Introduction

Conclusions

References

Tables

Figures



Back

Close

Full Screen / Esc

Printer-friendly Version

Interactive Discussion



A multi-site IWV techniques intercomparison

R. Van Malderen et al.

Title Page

Abstract

Introduction

Conclusions

References

Tables

Figures

◀

▶

◀

▶

Back

Close

Full Screen / Esc

Printer-friendly Version

Interactive Discussion



McCarthy et al., 2009) and hence also partially anticipate for the spatial inhomogeneity of radiosonde measurements. The use or development of such a homogenization procedure lies out of the scope of the present paper and the used IGRA database of radiosonde measurements therefore does not constitute a homogeneous dataset.

We nevertheless incorporate these RS measurements in our techniques intercomparison, as they have been widely used in such analyses in the literature so far (see e.g. Buehler et al., 2012) and they provide the longest record (up to 60 yr) of upper-air temperatures and humidity. Moreover, they have near-global coverage and high vertical resolution, are launched under all weather conditions, and daily daytime and nighttime observations take place at a large number of sites.

Independent uncertainty estimates of the IWV integrated from radiosonde profiles have not been reported in the literature so far, but Wang and Zhang (2008) concluded from comparisons with ground-based GPS measurements that the averaged systematic error for capacitive sensors, or their mean dry bias, is equal to -1.2 mm (-6.8 %) with a random error of 1.74 mm. Miloshevich et al. (2009) compared the IWV values calculated from the latest generation of Vaisala radiosondes (RS92) with microwave radiometer measurements and estimated a precision of 5 % for the IWV after applying an ultimate correction strategy.

2.4 GOME/SCIAMACHY/GOME-2

The “Global Ozone Monitoring Experiment” (GOME) on ERS-2, the “Scanning Imaging Absorption spectroMeter for Atmospheric CHartographY” (SCIAMACHY) on Envisat, and an updated version of GOME, GOME-2, on MetOp-A measure back-scattered light in the ultraviolet, visible and near-infrared parts of the electro-magnetic spectrum. Total water vapour column amounts are retrieved from the spectral measurements in the visible wavelength region at 608–680 nm based on Differential Optical Absorption Spectroscopy (DOAS) providing a global record of total water vapour column data since the GOME launch in 1995. Details on the MPI-C retrieval of water vapour columns can be found in Wagner et al. (2011).

A multi-site IWV techniques intercomparison

R. Van Malderen et al.

Title Page

Abstract

Introduction

Conclusions

References

Tables

Figures

◀

▶

◀

▶

Back

Close

Full Screen / Esc

Printer-friendly Version

Interactive Discussion



The ground pixel size of GOME is 40 km×320 km, 30 km×60 km for SCIAMACHY, and 40 km × 80 km for GOME-2. All satellites are operated in a sun-synchronous orbit, with a constant equator crossing time (local) around 10:30 (GOME), 10:00 (SCIAMACHY) or 9:30 (GOME-2). Global coverage is provided after 3 (GOME), 6 (SCIAMACHY) and 1.5 (GOME-2) days. In the remaining of the paper, we will use the acronym GOMESCIA to denote the three instruments GOME, SCIAMACHY, and GOME-2 at once.

Three main error sources contribute to the uncertainty of the GOMESCIA IWV retrievals (Wagner et al., 2011; EUMETSAT, 2010): (1) the errors of the spectroscopic data for the H₂O and O₂ absorptions are estimated to about 5–10 %; (2) the uncertainty of the spectral retrieval as determined from the spectral residual is typically < 3 %; (3) the dominant error source is caused by uncertainties of the atmospheric radiative transfer, mainly due to effects of varying cloud cover and surface albedo. This error source is estimated to be about 15 % for clear sky observations and up to 100 % for individual observations in the presence of large cloud amounts. This range of uncertainty was largely confirmed by extensive validation exercises (Schröder and Bojkov, 2012) within the GLOBVAPOR project (<http://www.globvapour.info/index.html>). Here it should be noted that measurements with the largest cloud contamination are filtered out using a threshold criterion for the simultaneously measured O₂ absorption (Wagner et al., 2006, 2011), see also Sect. 4.3.

Recently it was found (Schröder and Bojkov, 2012) that systematic biases between the time series of the different sensors can occur, although they were merged using coincident observations during the respective overlap periods. This especially applies to the transition from SCIAMACHY to GOME-2 in the beginning of 2007. For observations over the continents, these jumps are up to 4 mm. Detailed investigations indicate that the jumps are caused by the differences in ground pixel size and swath width. Activities are ongoing to eliminate these jumps in the next version of the GOMESCIA data set by only using similar pixel sizes and viewing geometries.

2.5 AIRS

The Atmospheric Infrared Sounder (AIRS) is a cross-track scanning instrument aboard the polar orbiting Aqua satellite launched by NASA on May 2002 (Aumann et al., 2003). The scans from AIRS correspond to ellipsoidal foot prints with a major axis varying from 13.5 km (at nadir) to 31.5 km. A full global coverage is obtained in half a day, so AIRS provides two soundings per day at a given location on Earth between 45° N and 45° S. The instrument itself is a hyperspectral, scanning infrared sounder based on a grating spectrometer, that measures emitted radiation in the range from 3.7 to 15 μm , with a spectral resolution ($\lambda/\Delta\lambda$) of 1200 (Aumann et al., 2003). Because of this high spectral resolution and excellent absolute accuracy, the AIRS retrieval algorithms are able to produce profiles of atmospheric temperature, moisture and trace gases, with a vertical resolution of a few kilometres throughout the troposphere. The AIRS IWV is obtained by integrating the vertical profile of water vapour mixing ratio retrieved from cloud-cleared radiances (Bedka et al., 2010, and references therein). The stated theoretical accuracy specification for the absolute AIRS total water vapour product is 5 % (Aumann et al., 2003). Fetzer et al. (2003) showed biases of -4 to 4 % absolute for full water vapour retrievals, in 2 km layers between the surface and 500 hPa, against Vaisala operational radiosondes over water. Also over (identical) ocean scenes, observational biases generally less than 5 % in IWV are again found by Fetzer et al. (2006), who compared the IWV observations of AIRS and AMSR-E (Advanced Microwave Scanning Radiometer – EOS, on board Aqua). A validation over land of AIRS version 4 retrievals of IWVs by measurements of more than 375 GPS receivers over the continental USA (from April to October 2004) is described in Raja et al. (2008). They concluded that the absolute biases between these two techniques range from 0.5 to 1.2 mm and RMS differences from 3 to 4.5 mm, with consistently large monthly correlation coefficients, ranging from 0.91 to 0.98.

This study examines AIRS level 2 version 5 moisture products, which are available from September 2002 onwards. We took into account the flag Qual_H2O for

AMTD

7, 1075–1151, 2014

A multi-site IWV techniques intercomparison

R. Van Malderen et al.

Title Page

Abstract

Introduction

Conclusions

References

Tables

Figures



Back

Close

Full Screen / Esc

Printer-friendly Version

Interactive Discussion



quality control of the IWV product. This flag is based on the lowest good estimation of the pressure P_{Best} , which depends on the cloud cover. The best data quality flag ($Qual_H2O = 0$) is assigned to the data if P_{Best} equals the surface pressure, $Qual_H2O = 1$ for those data where P_{Best} is lower than 300 hPa. If P_{Best} is higher than 300 hPa, the value 2 is attributed to the flag $Qual_H2O$. In this paper, we will only deal with retrievals for which $Qual_H2O = 0$ or 1.

3 Methodology

From the discussion in Sect. 2, we conclude that at current stage, the IWV derived from GPS is best suited for the analysis of trends, as it provides a long-term, worldwide (continental), homogeneously (re)processed and all-weather database of IWV values. That is the reason why we selected in this paper the IWV dataset derived from the IGS network as the reference w.r.t. which the observations of all other, co-located, techniques will be compared. In this section, we present the different aspects of the methodology we developed to make these comparisons.

3.1 Co-location criteria and site selection

As a first step, we searched into the IGS and AERONET sun photometer site databases for worldwide co-locations between both instruments with a maximal separating distance of 30 km. Additionally, we identified IGRA radiosonde sites with the same maximal separation distance criteria. Then, we extracted data from GOME/SCIAMACHY/GOME-2 and AIRS crossings at those selected sites. Because the ground pixel sizes of these different satellite devices are not equal, differences between the limiting distance between the pixel centre and an IGS station for co-location are admitted. The best compromise with other criteria like amount of co-locations, presence of clouds was found for a maximum distance of 50 km for AIRS and the inclusion of the IGS station in the satellite ground pixel for GOME/SCIAMACHY/GOME-2. We

A multi-site IWV techniques intercomparison

R. Van Malderen et al.

Title Page

Abstract

Introduction

Conclusions

References

Tables

Figures



Back

Close

Full Screen / Esc

Printer-friendly Version

Interactive Discussion



A multi-site IWV techniques intercomparison

R. Van Malderen et al.

Title Page

Abstract

Introduction

Conclusions

References

Tables

Figures



Back

Close

Full Screen / Esc

Printer-friendly Version

Interactive Discussion



will come back to this issue later in the paper, in Sects. 4.3 and 4.4 and Sects. 5.3 and 5.4. Finally, as already addressed in Sect. 2.1.2, the WMO database of synoptic stations was consulted to find co-locations with IGS stations within a maximal horizontal distance of 50 km. With these criteria, we compiled a list of 28 locations where we dispose of a co-location of an IGS station with at least one CIMEL sun photometer or a radiosonde launch site. A world map showing the locations of these 28 sites is presented in Fig. 2. The data availability as a function of time for the different instruments at the co-locations is shown in Fig. 3. Unfortunately, our co-location sites are all Northern Hemisphere sites² (see Fig. 2), with the strongest concentration in Europe, but nevertheless representing more or less the whole longitude band. From Fig. 3 it should be noted that there is no single station in our selection at which all instruments are represented for the entire time period. Furthermore, looking at Fig. 3, it seems justified to compare the IWVs from all devices with the coincident GPS-based IWV observations, as these latter provide a reasonable IWV time series for the majority of the selected stations.

3.2 Selection of synoptic stations for the ZTD-IWV conversion

To convert ZTDs to IWV values, the knowledge of coincident surface pressure and temperature observations is needed at the GPS site (see Sect. 2.1.1). As high-quality observations of these meteorological variables are rarely available at the GPS site, we rely on WMO synoptic station measurements in the vicinity. For about half (13) of the IGS stations in our selection, more than one WMO station lies within the imposed maximum horizontal distance of 50 km. Consequently, different strategies can be applied to make use of these multiple neighbouring WMO stations for the ZTD conversion at a given IGS station. For instance, Wang et al. (2007) average the pressure observations

²This is mainly because of the combination of our co-location criteria and the fact that the largest concentration of GPS, radiosonde and CIMEL sun photometer instruments is found in the Northern Hemisphere.

A multi-site IWV techniques intercomparison

R. Van Malderen et al.

Title Page

Abstract

Introduction

Conclusions

References

Tables

Figures

◀

▶

◀

▶

Back

Close

Full Screen / Esc

Printer-friendly Version

Interactive Discussion

(corrected for the altitude difference) of all selected synoptic stations using the inverse of their distance to the GPS station as the weight to obtain the pressure at the GPS station height and location. However, different synoptic data sources of deviating quality and at sometimes geographical distinct locations are then being mixed up. An alternative approach, followed in this paper because it better fulfils the aim of an “as purely observational as possible” techniques intercomparison, consists of selecting the “best” WMO station for a given IGS station. To define the “best” WMO station, different possible criteria could be taken into account: (1) the data quality of the WMO station, i.e. no apparent inhomogeneities, small number of outliers. . . , (2) the length and time frequency of the observation records, (3) the altitude difference w.r.t. the GPS station, (4) the horizontal separation distance to the GPS station, and (5) the resulting GPS IWV correspondence with co-located IWV observations measured by other techniques. So, as a first step, we checked the surface measurements of the SYNOP station to remove spurious time periods and outliers. Then, we analysed the impact of the height difference and horizontal separating distance on the calculated IWV values by creating, for a given IGS station, scatter plots between the IWV datasets calculated from the surface measurements provided by each of the co-located WMO SYNOP station.

We will give here two examples. First, for the IGS station FFMJ (located near Mainz, Germany, at an altitude of 130 m a.s.l.), three WMO stations are located within 50 km distance: 10532 (205 m a.s.l., at 36 km), 10635 (826 m a.s.l., at 29 km), and 10637 (113 m a.s.l., at 24 km), see Table 2. The station with WMO code 10637 has the smallest height difference and horizontal separating distance. So, we constructed IWV scatter plots based on observations from stations 10532 and 10635 w.r.t. IWV values calculated from the data of station 10637. The scatter plot properties are shown in Table 2.

It strikes that the large altitude difference between the IGS station and the WMO station 10635 cannot completely be corrected for, as a bias of 1.41 mm persists between the IWV values derived from the WMO stations 10635 and 10637 (this is the maximum bias found for all IGS and WMO stations considered in this paper). On the other hand, the scatter plot properties between the IWV values calculated from the WMO stations

10532 and 10637 show that the differences between both sets of IWV values obtained with the IGS station are really marginal: the bias equals to 0.08 mm with a RMS of 0.32 mm, the slope difference is only 0.002. So, for this IGS station we selected the WMO station 10637 as surface data source.

5 Another example is given by the IGS station SUWN, near Seoul in South-Korea, located at an altitude of 59 m a.s.l. Four possible WMO stations, all at a distance around 45 km from the IGS station and with height differences ranging from -21 m to 91 m, could be used for the ZTD-IWV conversion. Then, the IWV biases induced by using different WMO SYNOP stations range from -0.10 mm to 0.11 mm with a maximum
10 RMS of 0.49 mm and a maximum slope difference of 0.006. The values mentioned here are at the high-end range, so typical values are significantly lower for the majority of the other IGS stations with multiple co-located WMO stations.

Additionally, we also analysed differences in scatter plot properties between GPS IWV values calculated from different co-located WMO stations on one hand, and IWV values observed with co-located techniques on the other hand. So the selection of the final WMO station providing surface values for the ZTD-IWV conversion can also be assessed with the help of a co-located technique. Or, to put it in another way: with this analysis we also study the influence of the selection of the WMO station on the techniques intercomparison. To illustrate this, we return to the example of the IGS station
20 FFMJ, which is now compared with the co-located CIMEL sun photometer at Mainz (located at a distance of 28 km from the IGS station and an altitude of only 20 m higher), see Table 3. We note that the differences in scatter plot properties are of the same magnitude than the GPS IWV scatter plot differences and are almost insignificant for the IWV values generated from the WMO stations 10532 and 10637. In this case, the choice for the WMO station 10637, the closest station with minimum altitude difference,
25 seems justified, as also the RMS, correlation coefficient, and regression slope coefficient are slightly better. To be complete, we also want to mention that for the SUWN IGS station, the scatter plot properties of the different GPS IWV datasets with the co-located (20 km distance, 7 m height difference) RS site range between -0.22 mm and

A multi-site IWV techniques intercomparison

R. Van Malderen et al.

Title Page

Abstract

Introduction

Conclusions

References

Tables

Figures



Back

Close

Full Screen / Esc

Printer-friendly Version

Interactive Discussion



0.05 mm (bias), between 3.18 mm and 3.21 mm (RMS), between 0.922 and 0.927 (regression slope coefficient), and with identical correlation coefficients (0.982).

To summarize, for a given IGS station, we chose the WMO surface station with minimum altitude difference and at minimum distance (in this order). If another WMO station has a much larger data record, its surface data is used instead if the differences between the resulting IWV datasets are insignificant. So, for our selection of 28 IGS stations, the finally selected WMO surface stations, see Table 4, are located on average at a distance of 27.5 (± 11.1) km and the average absolute height difference amounts to 35.7 (± 42.2) m, with extreme values obtained for the IGS stations NISU and HLFX with the WMO stations located respectively 197 m below and 121 m above.

3.3 Techniques altitude difference correction scheme

Another issue that needs to be discussed is the altitude difference that might exist between the different co-located ground-based or in-situ instruments measuring IWV. This altitude difference will introduce at least an artificial bias between the IWV datasets compared, because the device that is located at the lower altitude should logically measure a larger column of water vapour, and hence larger IWV values. Luckily, height differences between ground-based and in-situ instruments at our selected sites are relatively small: the maximum height difference between the GPS antenna and the radiosonde launch site is at most 105 m (Munich, OBE2), and at most about 75 m (Munich, OBE2 and Paris, OPMT) between co-located GPS antenna and CIMEL sun photometers. However, we explored the possibilities of applying techniques altitude difference correction schemes and we investigated their impact on the techniques intercomparisons in this section.

For co-located IGS and radiosonde stations, the altitude correction is most easily applied to RS observations, because these of course provide vertical profile information. We make a distinction between two possible cases: for RS stations located below IGS sites, the vertical integration of RS specific humidity q is started at a pressure level corresponding to the IGS site altitude. The pressure at this level is computed from the

A multi-site IWV techniques intercomparison

R. Van Malderen et al.

Title Page

Abstract

Introduction

Conclusions

References

Tables

Figures



Back

Close

Full Screen / Esc

Printer-friendly Version

Interactive Discussion



A multi-site IWV techniques intercomparison

R. Van Malderen et al.

Title Page

Abstract

Introduction

Conclusions

References

Tables

Figures



Back

Close

Full Screen / Esc

Printer-friendly Version

Interactive Discussion



heights of the IGS and RS sites based on the hydrostatic equilibrium hypothesis. At the starting pressure level, q is obtained by linear interpolation of the RS data. On the other hand, for RS stations located above IGS sites, RS surface data are extrapolated hydrostatically with an assumed temperature lapse rate of -6.5 K km^{-1} , while q is extrapolated by assuming that the dewpoint temperature depression (temperature minus dewpoint temperature) is constant with height, as explained by Deblonde et al. (2005). An alternative approach was proposed by Buehler et al. (2012), who found a relative bias $\Delta \text{IWV}/\text{IWV}$ of -3.5% per 100 m altitude difference. This number was obtained by simply starting the IWV integration of the radiosonde data of the Arctic station Esrange at different altitudes in order to simulate what a sensor at different altitudes should report as IWV value. However, the actual scaling factors seem to depend on location (for example, Bock et al., 2007, found a value of -4.0% per 100 m for Africa) and might therefore not generally applicable to other IWV data.

Correcting the CIMEL IWV data for the altitude difference with a co-located GPS station is not as straightforward. The only possible altitude difference correction might then be applied to the GPS IWV data instead. In particular, we applied a ZHD correction (ΔZHD) – a dry/hydrostatic bias correction – to account for the pressure difference between the CIMEL and GPS sites (see Eq. 2):

$$\Delta \text{ZHD} = (0.0022768 \pm 5 \cdot 10^{-7}) \cdot (P_s - P_{\text{CIMEL}}) / (1 - 0.00266 \cos 2\varphi - 0.00000279 \cdot h) \quad (5)$$

The pressure at the CIMEL site, P_{CIMEL} , is, as is P_s , calculated with the hydrostatic and ideal gas equations from the surface pressure recorded at the synoptic station. This correction is then added to the ZHD and converted to IWV as explained in Sect. 2.1.1. If the altitude of the GPS station is higher than the altitude of the CIMEL site, then $P_s < P_{\text{CIMEL}}$ and $\Delta \text{ZHD} < 0$. The corrected ZHD will then be smaller than the uncorrected ZHD, but the corrected ZWD will be larger than the uncorrected ZWD (see Eq. 1), leading to a higher corrected IWV at the lower altitude CIMEL site (see Eq. 3).

As a consequence, methods exist to correct the IWV values for an altitude difference between the ground-based and in-situ techniques. However, in this paper, we only

A multi-site IWV techniques intercomparison

R. Van Malderen et al.

Title Page

Abstract

Introduction

Conclusions

References

Tables

Figures



Back

Close

Full Screen / Esc

Printer-friendly Version

Interactive Discussion



applied the altitude difference correction scheme for the radiosonde IWV retrievals, because of several reasons. First of all, we prefer to have the same common reference GPS IWV data for the comparison with the other techniques: we want to avoid applying a correction to this data when compared to the CIMEL data, and no correction when comparing with the satellite IWV retrievals. Secondly, reducing the RS IWV data to the GPS station altitude really improves the GPS-RS IWV comparisons: the (mean) biases and RMS are reduced, and higher (mean) scatter plot correlation coefficients are obtained. The only exception is that the regression line slope coefficients deviate more from unity after RS IWV correction. The correction also does not introduce a dependence of the GPS-RS IWV scatter plot properties on the GPS-RS altitude differences. Unfortunately, the opposite is true for the altitude correction applied to the GPS IWV retrievals for comparison with co-located CIMEL sites, whereas before correction, there was no clear correlation between the IWV biases between both techniques and the altitude difference of both sites. Furthermore, we cannot detect a real improvement in the coincident GPS-CIMEL IWV comparisons after adopting the altitude correction strategy to the GPS IWV retrievals.

3.4 Coincidence criteria

So far, we spoke about the concept of “coincident” measurements. In this section, we will elaborate on the precise meaning of “coincident”. First of all, during the ZTD to IWV conversion, “coincident” observations of surface temperature and pressure of a co-located WMO station were used. For this particular case, as the time frequency of the GPS-based ZTDs is very high (every 5 min), SYNOP observations at exactly the same time i.e. within 1 min, were used. The time frequency of the resulting GPS IWV values is then mostly driven by the time frequency of the SYNOP observations, unless the GPS ZTD time series has significant gaps.

Then, for creating the IWV scatter plots, “coincident” measurements of two considered techniques are needed. We again emphasize that for these scatter plots “coincident” should be interpreted in the strictest sense, because we will not apply any time

A multi-site IWV techniques intercomparison

R. Van Malderen et al.

Title Page

Abstract

Introduction

Conclusions

References

Tables

Figures

⏪

⏩

◀

▶

Back

Close

Full Screen / Esc

Printer-friendly Version

Interactive Discussion



averaging nor interpolation. Instead, all comparisons shown are point-by-point comparisons, which means that every IWV measurement of a given instrument (RS, CIMEL, GOMESCIA and AIRS) will be compared with the corresponding GPS IWV value, within a maximal time interval of 10 min for the CIMEL instrument, and 30 min for radiosondes, GOME(2)/SCIAMACHY and AIRS. When a measurement of an instrument coincides with several GPS IWV values within these time intervals, we use exclusively the coincidence with the minimal time difference. This strategy reflects the scope of the present paper to make a techniques intercomparison, based on purely observational data. We also compared hourly averages and the results obtained from that analysis are identical to the ones presented here. The difference between the applied time intervals for defining “coincident” data for the selected instruments stems from the different temporal resolution of these instruments: under clear-sky conditions, the CIMEL instrument measures every 15 min, whereas the balloon at which the radiosonde is attached, needs at least half an hour to traverse the troposphere and hence measure most of the water vapour column. The GOME(2)/SCIAMACHY and AIRS measurements are also more instantaneous observations of the IWV, but data is only available once or twice a day above a specific location, and under (almost) clear sky conditions. Here we chose the 30 min time interval to incorporate a significant number of “coincident” GOMESCIA/AIRS and GPS IWVs, because a large number of IGS IWV time series have a temporal resolution of at most 1 h due to the low temporal resolution of the available WMO meteorological data. Once again, we stress that the length of the time interval for defining coincident observations does not influence the conclusions reached in the paper.

4 Case study: a focus on Brussels, Belgium

To demonstrate the methodology used for the techniques intercomparison, we first focus on the IWV databases gathered at Uccle, Brussels, Belgium (IGS station BRUS, 50°48′ N, 4°21′ E, 100 m a.s.l.). We have several reasons to concentrate first on this IGS

A multi-site IWV techniques intercomparison

R. Van Malderen et al.

Title Page

Abstract

Introduction

Conclusions

References

Tables

Figures



Back

Close

Full Screen / Esc

Printer-friendly Version

Interactive Discussion



station. First, all ground-based instruments used in this study are exactly co-located at the same site at Uccle. It is also the case for the weather station providing the necessary meteorological data for the ZTD to IWV conversion. So, for Brussels we do not have to take into account any height difference nor separation distance between the different instruments! Secondly, several meteorological data (e.g. the cloud cover) collected at Uccle (location of the Royal Meteorological Institute of Belgium) provide additional information for the interpretation of IWV differences between different instruments: these can e.g. clarify if meteorological conditions have an impact on the performances of the different datasets. Thirdly, we dispose of all metadata of each of the ground-based devices operated in Brussels, so that we are aware of any instrumental change that might give rise to an inhomogeneity in the instrument's IWV time series.

An overview of all available IWV datasets in Brussels is shown in Fig. 4. A first consideration to make about this figure is the presence of the well-established seasonal cycle in the IWV time series: maximum values are reached during the summers (June–August), when the surface temperatures are highest, and minimum values are attained during the winters (December–February). Furthermore, it should be obvious from this figure that the different instruments cover different observation periods. Rather than determining a time period covered by all instruments, we selected a reference instrument against which the other techniques will be compared for the longest time interval possible, as already explained in Sect. 3. From Fig. 4, it should be obvious that the choice of the GPS instrument as reference instrument in the case of the Brussels station is certainly justified, based on the following reasons: (1) BRUS ZTDs provided by IGS has a time frequency of 5 min, but the automatic weather station at Uccle (needed for the ZTD-IWV conversion), does measurements every 10 min, so that the resulting time frequency of GPS IWVs is 10 min, (2) the launch of the automatic weather station at the end of 1999 also marks the beginning of the data availability at this high temporal resolution (the IGS site in Uccle, BRUS, is operated continuously by the Royal Observatory of Belgium since 1993), which is sufficiently long compared to the other techniques,

and (3) the GPS ZTD time series only have minor data gaps. We also mention that, since GPS ZTDs are provided thanks to the reprocessing efforts carried out by the IGS, a homogeneous dataset is guaranteed.

So, in the remaining of this section, we will present scatter plots of coincident IWV values from a given device w.r.t. GPS.

4.1 CIMEL sun photometer

The CIMEL sun photometer was installed in Uccle, Brussels, in July 2006 by the Belgian Institute of Space Aeronomy. It measured continuously since then, with the exception of calibration periods (prerequisite of being part of AERONET). These periods are 11 September 2007–3 March 2008, 4 May 2009–9 July 2009, and 13 September 2010–3 December 2010. The excellent performance of this CIMEL instrument has already been tested for the aerosol optical depth retrievals by comparison with the co-located Brewer spectrophotometer Aerosol Optical Depth observations (De Bock et al., 2010). Here, CIMEL IWVs are compared with IWVs of the IGS site “BRUS”. The resulting scatter plot of more than 9000 coincident observations can be found in Fig. 5. A very good agreement (the linear Pearson correlation coefficient is above 0.99) is found between both techniques and the average bias amounts to only 0.17 mm. Also, the RMS has a very low value of only 0.95 mm, reflecting the negligible dispersion in the scatter plot. On the other hand, the slope of the linear regression line has a value significantly lower (0.915 ± 0.001) than the ideal one-to-one correlation. As can be derived from Fig. 5, the cause for this too low slope value is twofold: (1) at low IWV values (< 10 mm), the CIMEL IWVs are always higher than the corresponding IGS IWVs, and (2) at high IWV values (> 30 mm), the IGS IWVs are higher than the corresponding CIMEL observations. The first cause can be attributed to the fact that, under dry conditions, the GPS data are known to be less precise (Wang et al., 2007). The second effect might reflect the observation bias present in the CIMEL data: the CIMEL instrument needs a clear sky in the direction of the sun. At high IWV values, there is a higher probability to have clouds. Water vapour associated with these clouds might be captured by GPS signals,

A multi-site IWV techniques intercomparison

R. Van Malderen et al.

Title Page

Abstract

Introduction

Conclusions

References

Tables

Figures



Back

Close

Full Screen / Esc

Printer-friendly Version

Interactive Discussion



but never by the CIMEL sun photometer, so that the CIMEL IWVs will always be lower than the corresponding IGS IWVs in these cases.

4.1.1 Influence of clouds

To test the impact of the cloud cover on our intercomparisons, we analysed the cloud meteorological data at the epochs of the coincident GPS-CIMEL IWV values. We end up with a total of about 1100 coincident IWV and cloud cover observations. The cloud meteorological dataset consists of a classification of the cloud cover into different classes, ranging from 0 (clear sky) to 8 (sky totally covered with clouds), the so-called “octas”. As we want to study the influence of the cloud cover on the GPS-CIMEL IWV scatter plots, we combine several of these “octa” classes to have a representative number of observations for each “combined” class. Otherwise, the effect that the number of the observations has on the scatter plot properties cannot be ruled out. As can be seen on Fig. 6, we constructed scatter plots and linear regression lines for IWV values under clear sky conditions, under very low cloud cover (“octas” equal to 1 or 2) and under moderate to heavy cloud cover (“octas” larger than 2). First of all, it should be noted that the (mean) IWV values observed by both the CIMEL and the GPS increase with increasing cloud cover. Gaffen and Elliott (1993) found that especially over the continents in mid and high latitudes, the total column precipitable water is systematically lower for clear sky conditions compared to cloudy scenes. So, this is confirmed by our small analysis for Brussels. Secondly, whereas the CIMEL minus GPS IWV bias is positive for very low or no cloud cover, it becomes negative for high cloud cover. So, for increasing cloud cover, GPS is measuring more frequently higher IWV values than the CIMEL sun photometer does. We believe that this is due to the fact that under such meteorological conditions, the (zenith) IWV values observed by GPS is incorporating contributions from clouds while observing in slant directions towards the different satellites. The CIMEL observation on the other hand, is always a cloud-free measurement solely in the solar direction. Thus, the only contribution from clouds might be in the air mass measurement, needed to convert the solar slant measurements to the zenith

A multi-site IWV techniques intercomparison

R. Van Malderen et al.

Title Page

Abstract

Introduction

Conclusions

References

Tables

Figures



Back

Close

Full Screen / Esc

Printer-friendly Version

Interactive Discussion



values. As a consequence, the higher range of GPS IWVs for more cloudy skies give rise to lower regression line slope coefficients of the GPS-CIMEL scatter plots, caused by the observation bias of the CIMEL instrument. That is why we believe that the rather low slope value of the regression line in the overall Brussels GPS-CIMEL scatter plot (see Fig. 5) can be attributed to the observation bias of the CIMEL instrument.

4.1.2 Solar slant integrated water vapour measurements

In the previous Sect. 4.1.1, we developed a hypothesis on the contribution of clouds to IWV measurements in different slants, but based on differences observed between slant measurements mapped in the zenith direction only. As the CIMEL and GPS retrievals use different strategies to convert the measurements from slant directions to zenith, we should check the influence of these strategies on the GPS-CIMEL IWV comparison. One way forward is to compare coincident IWV values in the direction of the Sun (the so-called solar slant IWV). These solar slant IWVs are one step back in the data process to obtain IWVs from the slant transmittance measured by the CIMEL sun photometer and can be obtained easily by multiplying the (zenith) IWVs with the optical air mass as defined in Kasten and Young (1989) (standard CIMEL data processing). These CIMEL solar slant IWVs should then have no contributions from clouds, by definition.

To convert GPS IWVs into solar slant IWVs for Sun elevations higher than a cut off angle of 7° , we used the same wet mapping function as the one used during the IGS data analysis, i.e. the wet GMF mapping function of Boehm et al. (2006) for the ZTD contribution and the horizontal gradients developed by Chen and Herring (1997).

If we now compare the GPS-CIMEL zenith and solar slant IWV scatter plots (Figs. 5 and 7), we find a somewhat smaller correlation, and a significantly higher bias and RMS for the solar slant IWVs. We further note that the regression slope deviates more from unity for the case of the solar slant IWV values (0.890 vs. 0.913), but this lower regression slope is strongly influenced by a small amount of high-range values, so it is imprudent to draw too strong conclusions from this feature. Certainly, this scatter

A multi-site IWV techniques intercomparison

R. Van Malderen et al.

Title Page

Abstract

Introduction

Conclusions

References

Tables

Figures



Back

Close

Full Screen / Esc

Printer-friendly Version

Interactive Discussion



plot comparison shows that there might be an impact of the different mapping functions used for the GPS and CIMEL IWV data conversion on the resulting scatter plots properties.

4.2 Radiosondes

5 During the period of our techniques intercomparison, three different radiosonde types were used at Uccle (see Fig. 4): the RS80 (until August 2007), the RS90 (November 2001–October 2003) and the RS92 (from September 2007), all produced by Vaisala. However, as the humidity sensors of the types RS90 and RS92 are identical besides some improvements in sensor design to e.g. minimize the solar radiation
10 heating, we will treat these two radiosonde types as one class, named RS9x. Both widely used radiosonde types RS80 and RS9x suffer from a well-known dry bias in their humidity measurements, although this bias is caused by different error sources: the chemical contamination and sensor ageing for the RS80 (see Sect. 2.3 and Van Malderen and De Backer, 2010, and references therein) and the solar radiation error
15 for daytime RS9x observations (Vömel et al., 2007). The RS80 humidity measurements at Uccle were corrected by the method developed by Leiterer et al. (2005), which is currently the best available correction scheme for this radiosonde type (Suortti et al., 2008). Nighttime sounding data exist for the RS90, and for the RS80 until November 2001. For all these radiosonde types, we dispose of data points every 10 s, so
20 that the theoretical vertical resolution is about 100 m on average, which is much higher than the best resolution provided by the IGRA database (data points at the standard and significant levels).

Rather remarkably, a wet IWV bias for both types of radiosondes is observed w.r.t. GPS: 0.41 mm for RS80 and 0.63 mm for RS9x. In both cases this wet bias is primarily caused by the nighttime observations: measurements carried out at 12:00 UTC
25 lead to a dry bias of 0.06 mm (1073 coincident data points) and a wet bias of 0.32 mm (901 data points) for the RS80 and RS9x radiosondes respectively, while the wet biases amount to 1.53 mm (449 data points) and 1.11 mm (596 data points) respectively for the

A multi-site IWV techniques intercomparison

R. Van Malderen et al.

Title Page

Abstract

Introduction

Conclusions

References

Tables

Figures



Back

Close

Full Screen / Esc

Printer-friendly Version

Interactive Discussion



A multi-site IWV techniques intercomparison

R. Van Malderen et al.

Title Page

Abstract

Introduction

Conclusions

References

Tables

Figures

◀

▶

◀

▶

Back

Close

Full Screen / Esc

Printer-friendly Version

Interactive Discussion



measurements carried out at 00:00 UTC. Another interesting finding is that the newest version of radiosondes, the R9x, really brings improvements in the IWV measurements (w.r.t. the RS80) when compared to coincident GPS IWV values: the correlation is better, the slope of the linear regression line is closer to unity, and the dispersion around the one-to-one correlation is lower by about one third. If we now compare the scatter plot properties for the daytime and nighttime radiosonde launches, we can draw the conclusion that, regardless the radiosonde type used, the correlation with coincident GPS IWVs is better for daytime observations (higher correlation coefficients, lower data variability) than for nighttime observations, but with higher regression slope coefficients (even higher than 1) and closer to unity for the nighttime observations. So, the radiosonde humidity sensors behave distinctly different in daytime and nighttime (because the GPS IWV retrieval should be in principle insensitive to the diurnal cycle). We suspect the heating of the humidity sensor by the solar radiation to be responsible for this daytime–nighttime difference. Threading the daytime and nighttime observations together and comparing this mixture of observations, done with even different humidity sensor types, with other devices, as we did in Fig. 5, should then be taken with caution. However, for this techniques intercomparison study, we will nevertheless treat them together, as usually found in the literature.

4.3 GOMESCIA

For these nadir observing satellites in the visible part of the spectrum, we start with the H₂O volume column density measurements of all pixels within a maximum distance of 300 km between the pixel centre and the IGS station, during an overpass of the IGS station. The goal is to start with a broad range of measurements and then reduce them to one single measurement per overpass, based on different criteria like distance, scan angle, and cloud information in terms of the observed O₂ column density. This reduction process is led by the comparison (scatter plot properties) with coincident IWV retrievals (i.e. within 30 min) at co-located IGS stations. We will describe this first here for the station BRUS and come back to it later in the world-wide exploitation

A multi-site IWV techniques intercomparison

R. Van Malderen et al.

Title Page

Abstract

Introduction

Conclusions

References

Tables

Figures

◀

▶

◀

▶

Back

Close

Full Screen / Esc

Printer-friendly Version

Interactive Discussion



of the GOMESCIA and IGS co-locations, in Sect. 5.3. First of all, we selected only the GOMESCIA measurements for which the ground pixel includes the BRUS IGS station. We found that this criterion alone did not lead to a good agreement with the coincident GPS retrievals: a high negative bias of more than 2 mm, with a RMS of almost 5 mm, and a correlation and regression slope coefficient around 0.75 and 0.65 respectively. It turned out that the normalized O_2 column density, which is used in the MPI-C to determine a cloud flag, is the parameter with the largest impact on improving the comparison with the co-located GPS IWV retrievals. A value of 1 for this flag is the applied threshold for cloud detection; higher values mean higher O_2 column densities, i.e. less cloud cover. Lower values can be caused by cloud shielding, but also by high mountains (of course not for the BRUS station). We could confirm the necessity of omitting the observations with a cloud flag below 1 for finding a satisfactory agreement with the GPS IWV measurements: the bias decreases now to -0.51 mm, the RMS to 3.72 mm, while the correlation coefficient and regression slope increase to resp. 0.866 and 0.825 (see Fig. 5). Alternatively, we tested several other approaches to reduce the different overpass measurements to one single measurement, but all imposing a lower limit of 1 for the (normalized) O_2 column density. Instead of demanding that the IGS station is located in the satellite ground pixel, we can select the measurement of the pixel with minimum distance between the IGS station and the satellite ground pixel centre and additionally imposing an upper limit for this distance. This strategy has the advantage that it does not favour the satellite devices with the largest pixel sizes (GOME), as the previous described method does. In any case, the scatter plot properties of this selection criterion are very similar to the “IGS station in pixel” criterion, but of course depend on the limiting distance: the smaller the limiting distance, the lower the RMS and the higher the correlation coefficient. The latter is a general finding, because it also applies to other selection criteria used in combination with this limiting distance (like simple or weighted averaging, maximum value for the cloud flag, etc.). The effect of limiting the satellite scan angle in the measurement reduction process on the GPS-GOMESCIA scatter plot properties is less significant as compared to limiting the distance. If the O_2

A multi-site IWV techniques intercomparison

R. Van Malderen et al.

Title Page

Abstract

Introduction

Conclusions

References

Tables

Figures

◀

▶

◀

▶

Back

Close

Full Screen / Esc

Printer-friendly Version

Interactive Discussion



column densities are further constrained, the slope of the GPS-GOMESCIA regression increases. If for instance, we select the GOMESCIA measurements with the maximal O_2 column density (superior to 1), i.e. we select the “best” cloud free value, the GPS-GOMESCIA regression slope increases to around 0.86. However, this criterion might introduce for some stations systematic biases due to spatial sampling as observations for higher O_2 columns (caused by less clouds or lower surface elevation) are favoured. This is not the case for Brussels, but occurs for stations at coastal areas (e.g. Marseille, France) or in hilly or mountainous regions (e.g. Munich, Germany) where a clear geographical dependence of the selected pixels could be detected when using this criterion.

To conclude, we will use the combination of the two criteria (IGS station in satellite ground pixel and cloud flag above 1) to reduce the different overpass measurements to a single measurement. So, the discussion in the remaining of this section will be based on those single overpass values. Compared to the scatter plot properties obtained between the GPS IWV retrievals and the ground-based and in-situ devices, the GPS-GOMESCIA scatter plot for Brussels, see again Fig. 5, exhibits a larger scatter and worse correlation, with a smaller linear regression slope coefficient. Of course, this worse agreement with the GPS IWV can be explained by the larger challenges that satellite IWV retrieval has to face compared to their ground-based or in-situ counterparts: the cloud cover issue, the reduced sensitivity in the lower tropospheric layers, a gridded dataset with issues on the pixel size, etc.

We will go a little more into detail in this last point. Our GOMESCIA dataset is composed of measurements with three different instruments, though using the same technique to retrieve the data from the measurements in the visible spectral range from 608 to 680 nm. Large differences in the ground pixel sizes exist between those three satellite devices, especially between GOME and SCIAMACHY/GOME-2. We therefore first investigate whether the ground pixel size has a large impact on the agreement with the co-located IGS IWV retrievals and hence, if a further splitting up of the data is required. We will do this analysis on the single overpass IWV values. As can be seen

A multi-site IWV techniques intercomparison

R. Van Malderen et al.

Title Page

Abstract

Introduction

Conclusions

References

Tables

Figures

◀

▶

◀

▶

Back

Close

Full Screen / Esc

Printer-friendly Version

Interactive Discussion



surprisingly, the best agreement with the GPS IWV measurements (and in particular with the slope coefficient closest to one) is obtained for the GOMESCIA observations in the high range end of the O_2 absorption, hence the most cloud free observations. As was the case for the CIMEL observations, measurements done at partly cloudy skies lead to lower regression slopes, higher RMS, lower correlation coefficients and the turnover from a positive to a negative bias. While for the CIMEL observations, we ascribed this change in the scatter plot properties (in particular the regression slope) to an observation bias of this instrument – always clear sky needed in the solar slant, in contrast to possible contributions from clouds to the GPS IWV values under partly cloudy skies – this observation bias is clearly not the cause for the behaviour of the GOMESCIA comparison with GPS in function of the cloud cover. Indeed, we should keep in mind that GPS IWV measurements are based on samples of the atmosphere forming a cone, where the projected area on the ground is increasing with height at a rate determined by the specified elevation cut-off angle. The measured values are thus representative for some 100 km^2 (Hagemann et al., 2003), which is much smaller than the GOMESCIA pixel areas ranging from 1800 (SCIAMACHY) to $128\,000 \text{ km}^2$ (GOME). As a consequence, cloud contributions in the GPS cone should be covered by the satellite measurements as well and we cannot use the same observation bias argument as in the CIMEL case. On the contrary, we assume that the worse agreement with GPS IWV observations under less clear sky conditions is caused by either an inferior data quality of the GOMESCIA IWV retrievals and/or the fact that the lower part of the atmosphere is not sensed by the satellite device under such conditions. In this context, we also want to address that the mean of the GOMESCIA IWV values is higher for mostly cloud free conditions (for cloud flag above 1.07, the mean IWV being 15.1 mm) compared to more cloudy scenes (cloud flag below or equal to 1.07, mean IWV equal to 13.3 mm), opposite to the means of the corresponding GPS-based values that decrease with decreasing cloudiness. This might actually point to the fact that the lowermost tropospheric layers are not sensed for less cloud-free scenes.

4.4 AIRS

For AIRS, we selected the closest pixel to the IGS station (in this case BRUS), with a maximum distance of 50 km between pixel centre and the IGS station, that passed the quality check (i.e. Qual_H2O flag values equal to 0 or 1, as already mentioned earlier). Then, at Brussels, looking for coincident (i.e. within 30 min) and those co-located AIRS and GPS IWV values resulted in an amount of almost 4500 data points, which are presented in the scatter plot of Fig. 5. The overall bias between AIRS and GPS is very small, only 0.01 mm, but at the cost of a rather high RMS of 3.51 mm. The correlation coefficient is equal to 0.883, which is in the same range as the one achieved for the other studied satellite device, GOMESCIA. Also the slope coefficient of 0.842 is comparable to the one found for GOMESCIA, and therefore probably also at least partially reflecting the cloud cover issues that satellite measurements of IWV have to deal with. Contrary to e.g. Bedka et al. (2010), we do not apply any site-dependent filtering of the AIRS retrieved data, but chose to study the impact of the Qual_H2O flag and the maximum distance between the IGS site and the AIRS pixel centre on the GPS-AIRS scatter plots.

First, we restricted the AIRS retrievals to the data points that have the best flag Qual_H2O = 0. Besides a reduction of the available data points for the techniques intercomparison to about a ninth of the original number, see Fig. 10, we found an increase of the bias to about 1.24 mm between AIRS and GPS for this subset of the data. This means that for the data with Qual_H2O = 0 (or the lowest good estimation of the pressure being the surface pressure) the AIRS IWVs are, on average, higher than the GPS IWVs. The reason for this is not very clear. As a consequence, the AIRS IWVs with Qual_H2O = 1 (PBest < 300 hPa) leads to underestimated IWV retrievals w.r.t. the GPS values, likely due to an underestimation of the contribution of the lower tropospheric layers to the total column water vapour content. On the other hand, limiting our AIRS dataset to the best data quality for the water vapour retrievals improves the scatter plot w.r.t. the GPS IWV data in two aspects: the correlation coefficient increases

AMTD

7, 1075–1151, 2014

A multi-site IWV techniques intercomparison

R. Van Malderen et al.

Title Page

Abstract

Introduction

Conclusions

References

Tables

Figures



Back

Close

Full Screen / Esc

Printer-friendly Version

Interactive Discussion



A multi-site IWV techniques intercomparison

R. Van Malderen et al.

Title Page

Abstract

Introduction

Conclusions

References

Tables

Figures

◀

▶

◀

▶

Back

Close

Full Screen / Esc

Printer-friendly Version

Interactive Discussion



considerably (to 0.921) and the RMS decreases. It has no effect on the slope of the linear regression, but the standard deviation for this slope coefficient increased by more than a factor of 2. This finding is contrary to the impact the cloud flag of the GOMES-CIA data had on the GPS-GOMES-CIA scatter plots. This could point to the fact that the AIRS H₂O quality flag is not very restrictive w.r.t. the cloud cover.

As a second test, we increased the maximum distance between the IGS station and the AIRS pixel centre to 100 km. As could be expected, this has a negative impact on the GPS-AIRS scatter plot properties: higher RMS, lower correlation coefficient and a lower slope. We also found a lower, even negative bias, between the AIRS and GPS IWV retrievals, hence the AIRS instrument underestimates, in the mean, the IWV w.r.t. the co-located GPS device. This can be explained by a larger contribution from Qual_H2O = 1 data.

Bedka et al. (2010) reported a significant nighttime dry bias in the AIRS retrievals at IWV values above 20 mm for one of their sites and suggested that this bias exists on a significant spatial scale over the US Great Plains and desert Southwest, but not in the Eastern United States or Canada. Fetzer et al. (2005) found an absolute bias of 0.5 mm in the IWVs retrieved by AIRS and AMSR-E during nighttime, but no bias during daytime observations. They attributed this daytime–nighttime difference to increased stratus clouds at night which have deleterious effects on the AIRS retrievals. We also looked at the differences between the nighttime and daytime AIRS observations w.r.t. the GPS IWV retrievals and classified AIRS overpasses as daytime when its solar zenith angle is lower than 90°. For Brussels, the nighttime AIRS IWV data seem to suffer from a small wet bias w.r.t. the GPS IWV retrievals (about 0.8 mm), whereas the daytime measurements show a dry bias (0.85 mm). Also the mean value of the coincident nighttime IWV retrievals is higher than its daytime counterpart. On the other hand, the AIRS nighttime observations show a better correlation with the GPS IWV retrievals (higher correlation coefficient, lower RMS), but the regression slope between the daytime observations is closer to 1 (but with a higher sigma of this slope). As there are generally two AIRS overpasses a day at Brussels, one daytime and one nighttime,

the samples of daytime and nighttime GPS-AIRS scatter plot data have about the same size, so that the scatter plot properties are not influenced by any sampling size effect.

4.5 Summary for Brussels

The Brussels scatter plot properties of the different techniques w.r.t. the GPS IWV retrievals are summarized in Table 5. We repeat here shortly the most important conclusions for the Brussels case study. First, the mean bias between the different techniques and GPS varies between -0.64 mm (SCIAMACHY) and $+0.61$ mm (RS9x). These are very small numbers, taking the instrumental and algorithm uncertainties of the different instruments into account. Secondly, the best correlation and lowest scatter of the data points are reached for the CIMEL vs. GPS comparison. On the other hand, the slopes of the regression lines w.r.t. the GPS IWV retrievals are closer to one for the all-weather device (RS) than for instruments demanding at least a partly clear sky (CIMEL, GOMESCIA, AIRS). When selecting only clear sky observations, these slopes increase for CIMEL and GOMESCIA, but hardly change for AIRS. Looking back at Fig. 5, we can note that, under dry conditions, the GPS is less sensitive to low IWV values than the other devices, which is in agreement with Wang et al. (2007). For low water vapour amounts, the ZTD is almost completely due to the ZHD. Therefore, small relative errors in these amounts produce a large relative error in their difference, i.e. in the ZWD and consequently in the retrieved IWV (Schneider et al., 2010).

The two satellite devices, although measuring water vapour in a different spectral window, reveal a similar agreement with the GPS IWV retrievals. We also could confirm that Vaisala's state-of-the-art radiosonde type (RS9x) compares better w.r.t. GPS IWV data than the preceding RS80 type. For both types, nighttime observations show a wet bias compared to daytime measurements and higher regression slopes. However, the overall correlation with the GPS IWV values is better for daytime measurements despite the apparent radiation dry bias. For AIRS, nighttime observations also exhibit a wet bias w.r.t. GPS IWV values and AIRS daytime observations, but in this case the nighttime observations agree best with the GPS IWV retrievals, despite the higher regression slopes

A multi-site IWV techniques intercomparison

R. Van Malderen et al.

Title Page

Abstract

Introduction

Conclusions

References

Tables

Figures



Back

Close

Full Screen / Esc

Printer-friendly Version

Interactive Discussion



for daytime AIRS measurements. Finally, as the GOME, SCIAMACHY and GOME-2 IWV retrievals behave similarly w.r.t. the coincident GPS IWV values, we will treat them as one dataset for the remaining of this paper.

In addition, for Brussels, we undertook for all instruments an intercomparison with GPS separately for different seasons. We found that for the considered scatter plot properties here, only the bias and the RMS show a clear, identical seasonal dependence for all instruments: the relative bias is minimal (or most negative) in summer, and maximal in winter, whereas the RMS is minimal in winter and maximal in summer. In this context, it should be noted that the largest mean IWV is obtained in Brussels in summertime and the smallest mean IWV in wintertime. Of course, this finding deserves further attention, but also should be analysed on a more global scale. Therefore, we will now extend our IWV techniques intercomparison to the selected 28 stations shown in Fig. 2.

5 World-wide exploitation of IWV datasets

With the methodology described in Sect. 3, we now convert for our selection of IGS stations (see Fig. 2) the ZTDs into IWV values with the help of the meteorological data of the chosen co-located WMO station (see Table 4). The radiosonde IWV data are reduced to the altitude of the co-located IGS station (see Sect. 3.3), whereas the CIMEL IWV data remain uncorrected. For the satellite IWV data, we will apply the data selection criteria (limiting distance between satellite ground pixel centre and IGS station and cloud cover flags) as explored for the Brussels case study. Finally, we created scatter plots similar to Fig. 5 for the selected sites for which we found instrumental co-locations with the GPS device. We stress again that for all the selected sites, we do not dispose of a co-location of the treated instruments, but at least of three of them out of five.

Before going into detail, for each technique separately, of the results obtained for the comparison with the GPS instrument, we already want to pay attention to the IGS

A multi-site IWV techniques intercomparison

R. Van Malderen et al.

Title Page

Abstract

Introduction

Conclusions

References

Tables

Figures



Back

Close

Full Screen / Esc

Printer-friendly Version

Interactive Discussion



A multi-site IWV techniques intercomparison

R. Van Malderen et al.

Title Page

Abstract

Introduction

Conclusions

References

Tables

Figures



Back

Close

Full Screen / Esc

Printer-friendly Version

Interactive Discussion



station BRMU. As it will be clear from the forthcoming figures and discussion, IWV values retrieved from the ZTD data from this station, are exposed to a large mean bias of the order of 5 mm compared to the coincident data of the other co-located techniques. We believe that the origin lies in the ZTD to IWV conversion, and more precisely in the used surface pressure data of the co-located WMO station with code 78016. Indeed, we found large deviations between the surface pressure data of this station and reanalysis surface pressure data for the pixels surrounding this station. Furthermore, a better agreement between the CIMEL data and the GPS IWV values at this station is reached if the latters are converted from the ZTD data using reanalysis surface pressure data. However, as our techniques intercomparison is meant to be purely observational, we keep the BRMU station in the selection, even if the IWV data is retrieved using suspicious meteorological data. This station might then be illustrative for the deviations caused by using wrong meteorological data in our analysis.

5.1 CIMEL sun photometer

Apart from some exceptions, for instance for the station KSTU, a good agreement is achieved between the two ground-based devices for the considered stations, see Fig. 11. As the GPS-based IWV values measured at the station KSTU compare well with the IWV data retrieved with GOMESCIA and AIRS, we presume that the CIMEL data of the station Krasnoyarsk have some data quality issues, although they are level 2 data. All regression slopes are inferior to 1, except for the scatter plot between BUCU and the CIMEL at Bucharest Inoe, for which a value of 1.01 is obtained. The regression slopes for the comparison of the same IGS station with two other CIMEL instruments are below 1. So, overall, the hypothesis that the weather observation bias is responsible for regression slopes below 1, as postulated in Sect. 4.1.1 for Brussels, seems valid on the global scale.

For the GPS-CIMEL comparisons, we dispose of seven IGS stations with more than one CIMEL instrument within the imposed limiting distance of 30 km. This gives us the opportunity to analyse for these co-locations directly e.g. the data quality and

A multi-site IWV techniques intercomparison

R. Van Malderen et al.

Title Page

Abstract

Introduction

Conclusions

References

Tables

Figures



Back

Close

Full Screen / Esc

Printer-friendly Version

Interactive Discussion



uncertainties of individual CIMEL instruments, the geographical dependency of the comparisons, etc. From those seven IGS stations, there are four stations (TLSE, VENE, OPMT, and BUCU) with a given CIMEL that has the largest difference in both the vertical and horizontal distance from the IGS station. In three of those cases (not BUCU), the data of this CIMEL agree worst with the GPS IWV values in all aspects (bias, RMS, R^2 and slope); for BUCU this CIMEL has only the largest deviation from unity in the regression slope coefficient. Among the three IGS stations (TLSE, VENE, and BRMU) with a CIMEL at the minimal vertical or horizontal distance, TLSE and VENE exhibit the best GPS-CIMEL agreement in all considered aspects. Clearly, the geographical aspect plays a role when comparing co-located CIMEL and GPS IWV values. Disentangling or even quantifying the effects of the vertical and horizontal distance on the GPS-CIMEL IWV scatter plots is not straightforward, as also other parameters (e.g. the number of coincident observations, the data quality of the measurements of each CIMEL) influence the quality of the scatter plots. In relative amounts, the bias and the RMS vary most among different GPS-CIMEL scatter plots, and also the regression slope changes considerably when comparing data of different CIMELs to the same GPS instrument. The correlation coefficient seems less sensitive to the chosen CIMEL with which the GPS IWV values are compared.

When we now consider the dataset of GPS-CIMEL scatter plots of all selected IGS stations, we do not find any correlation between the scatter plot properties at one hand and the altitude difference or distance between the CIMEL and GPS stations on the other hand. This finding strengthens us in the decision of not applying any altitude correction to the GPS IWV data when compared to a co-located CIMEL station. Quite surprisingly, correlations (with coefficients around 0.50) are discovered between the correlation coefficient and slope at one hand and the altitude of the station (either GPS or CIMEL) at the other hand, but these correlations are strongly provoked by the small correlation coefficients and slopes obtained for the IWV comparisons at the high-altitude station NISU. Furthermore, we could not detect any dependency of any of the scatter plot properties shown in Fig. 11 on latitude, longitude, or mean observed

IWV value. On the contrary, the RMS decreases with latitude and increases with mean observed IWV value. These latter two dependencies seem coupled and we will come back to them in Sect. 5.5.

5.2 Radiosondes

5 An overview of the scatter plot properties of the GPS-RS co-locations is provided in Fig. 11. The outlying station is now GLSV, with a large bias and RMS and small correlation coefficient and regression slope. The poor agreement between both devices is ascribed to the radiosonde data, as the GPS IWV data agree well with the IWV values retrieved from the CIMEL and the satellite instruments. Besides this outlier, the IWV
10 values given by co-located radiosondes and GPS device compare fairly well, but the regression slope coefficients are smaller than 1 for all stations.

In order to calculate IWV values from radiosondes, we integrated the specific humidity profile starting from the co-located GPS station height, as discussed in Sect. 3.3. When comparing the GPS-RS scatter plot properties for these altitude corrected RS
15 IWV values with these for the uncorrected RS IWV values, we found an improvement of the bias, RMS, and R^2 after correction for the majority of the stations, but lower regression slopes. However, the mean differences (weighted by the number of observations for each station) are very close to 0 for all properties. Moreover, we did not detect any correlation between the scatter plot properties and the height difference between the
20 RS and the GPS station, so that the application of both altitude corrections (depending on which station has the lowest altitude) seems justified for our sample of stations. For completeness, we also want to add that we could not observe a relationship between the distance between the RS and GPS station and any of the scatter plot properties.

Finally, there is neither a latitudinal (see Fig. 11) nor a longitudinal dependency of the
25 GPS-RS scatter plot properties bias, R^2 , and slope and we also could not establish any relation between these properties and the altitude or mean IWV value of the station. On the other hand, the RMS of the GPS-RS scatter plot decreases with latitude and increases with mean IWV. As the comparison of IWV values derived from RS or GPS

A multi-site IWV techniques intercomparison

R. Van Malderen et al.

Title Page

Abstract

Introduction

Conclusions

References

Tables

Figures



Back

Close

Full Screen / Esc

Printer-friendly Version

Interactive Discussion



measurements has been the subject of a considerable amount of studies (see e.g. the literature overview in Buehler et al., 2012), we will not go into further detail in this paper.

5.3 GOMESCIA

Looking at the GPS-GOMESCIA scatter plot properties, shown in Fig. 12, the first thing to note is the larger variability among the different stations compared to the other two discussed techniques so far. This larger variability is also clarified by the large RMS (error bars in the bias column bars), which lead to the poorer determination of the other scatter plot properties.

As for the Brussels case study, we tried different strategies to reduce all satellite overpass measurements above the IGS station to a single overpass value. And, as a matter of fact, exactly the same findings can be reached for the whole sample of stations – based on the averages of the scatter plot properties with weights equal to the number of coincident observations at a station – as for the Brussels case study. So, imposing a minimum value of 1 for the GOMESCIA cloud flag is really a requisite to obtain a satisfactory agreement between GPS and GOMESCIA IWV data pairs. Limiting additionally the distance between the satellite ground pixel centre and the IGS station has a positive impact on the means of the RMS and the correlation coefficient. Using other parameters to do the data reduction or filtering like the satellite scan angle hardly affects the means of the GPS-GOMESCIA scatter plot properties. Selecting the GOMESCIA measurements with a maximal O₂ column density increases to a large extent the mean of the GPS-GOMESCIA regression slope coefficients, but at the cost of introducing systematic biases due to the geographical dependence of the selection. For instance, in the case of the IGS station MARS (Marseille, France, a coastal station) we found that this methodology resulted in selecting the bulk of the pixels over the Mediterranean Sea. Also for the world-wide techniques intercomparison, we found a good GPS-GOMESCIA IWV agreement if the all overpass measurements were reduced to a single overpass value by imposing a lower limit of 1 for the O₂ column

A multi-site IWV techniques intercomparison

R. Van Malderen et al.

Title Page

Abstract

Introduction

Conclusions

References

Tables

Figures



Back

Close

Full Screen / Esc

Printer-friendly Version

Interactive Discussion



density and demanding that the IGS station falls in the satellite ground pixel, so these criteria will be used in the forthcoming discussion.

We will also elaborate more on the common treatment of the GOME, SCIAMACHY and GOME-2 IWV data for the entire sample of stations. Given the similar pixel sizes of SCIAMACHY and GOME-2, but a much larger pixel size for GOME, we compared the GPS-SCIAMACHY/GOME-2 scatter plots with the GPS-GOME scatter plots. Indeed, Noël et al. (2008) also concluded that the GOME-2 and SCIAMACHY water vapour total columns compare well on a global scale based on about seven months of data, although an indication for a small scan angle dependency was reported. As for the Brussels case study, we do not find any reason for treating those datasets separately, as the differences in the scatter plots w.r.t. GPS IWV values are very minimal. As a matter of fact, in the mean, the best agreement is found for the SCIAMACHY/GOME-2 and GPS IWV pairs, for all the discussed scatter plot properties, but the differences with the GPS-GOME scatter plot properties are minimal, except for the bias (-0.01 mm vs. 0.20 mm) and the slope (0.862 vs. 0.836). These better mean biases, RMS and correlation coefficients for SCIAMACHY/GOME-2 result from (weighted) averaging over all stations, of which half of them show those better scatter plot properties for SCIAMACHY/GOME-2, whereas higher slope coefficients for GPS-SCIAMACHY/GOME-2 regressions are reached for two third of the stations. Applying instrument dependent offsets in the IWV retrieval algorithms to homogenize the time series has a small positive effect on the averaged world-wide bias of less than 0.1 mm, and practically no effect on the other scatter plot properties.

Next, we will analyse the impact of fine-tuning parameters as the cloud flag and satellite scan angle on the GPS-GOMESCIA scatter plot properties of the selected locations at Earth. We therefore split for each station the GPS-GOMESCIA IWV pairs in two samples according to their observed O_2 absorption w.r.t. a chosen world-wide O_2 absorption threshold above 1. Subsequently, we compare the GPS-GOMESCIA scatter plot properties for the two dataset samples. We can conclude that selecting the most cloud free observations in a sample decreases the RMS and increases the

A multi-site IWV techniques intercomparison

R. Van Malderen et al.

Title Page

Abstract

Introduction

Conclusions

References

Tables

Figures

◀

▶

◀

▶

Back

Close

Full Screen / Esc

Printer-friendly Version

Interactive Discussion



A multi-site IWV techniques intercomparison

R. Van Malderen et al.

Title Page

Abstract

Introduction

Conclusions

References

Tables

Figures

◀

▶

◀

▶

Back

Close

Full Screen / Esc

Printer-friendly Version

Interactive Discussion



correlation and slope coefficients substantially, but at the cost of an increasing (absolute) bias. This statement holds both for the weighted means of these parameters as for the large majority of the stations. For the most cloud free observations, in general, the GOMESCIA instruments show a wet IWV bias w.r.t. the co-located GPS device, and a dry bias for less cloud free scenes. We also find that the mean IWV is lower for the most cloud free GOMESCIA measurements for especially the higher latitude stations, while the opposite is true for the low latitude stations. We should bear in mind that for high latitudes, no GOMESCIA observations are available in winter due to high SZA (see also Fig. 3). The high latitude stations also have a larger number of coincident GOMESCIA measurements with the GPS device under maximal cloud free circumstances compared to the number of measurements with lower cloud flag values (but still above 1). Decreasing the satellite scan angle improves especially the RMS and the R^2 of the GPS-GOMESCIA IWV scatter plots and the bias (not in absolute terms) with the GPS increases for almost all stations. The effect on the slope is more dependent on the stations considered and is therefore harder to catch on a more global scale.

Finally, we analysed the dependency of GPS-GOMESCIA bias and the coefficients of the correlation and the regression slope on the latitude (see Fig. 12), longitude, altitude, and mean IWV of the GPS stations, but we could not detect any geographical dependency of the scatter plots. Once again, the GPS-GOMESCIA RMS decreases with latitude and increases with mean IWV. Nevertheless, we can conclude that the GOMESCIA IWV retrieval methodology seems consistent over the entire globe.

5.4 AIRS

A summary of the GPS-AIRS scatter plot properties for the selected locations is given in Fig. 12. Small biases between the GPS and AIRS coincident IWV values exist, but with relatively high RMS. The correlation coefficients roughly range between 0.85 and 0.95, and all regression slope coefficients are smaller than 1, ranging between 0.70 and 0.95. This last finding is at least in qualitative agreement with the outcome of the GPS-AIRS comparison over the US undertaken by Raja et al. (2008) who concluded that,

A multi-site IWV techniques intercomparison

R. Van Malderen et al.

Title Page

Abstract

Introduction

Conclusions

References

Tables

Figures

◀

▶

◀

▶

Back

Close

Full Screen / Esc

Printer-friendly Version

Interactive Discussion



for mid-latitudes at least, the absolute values of AIRS derived total water vapour are dry biased in moist atmospheres ($IWV > 40$ mm) and wet biased in dry atmospheres ($IWV < 10$ mm). Comparing the scatter plot parameters w.r.t. GPS for the two considered satellite devices, it should be noted that there is less variability among the different stations for the AIRS device than for the GOMESCIA instruments.

The GPS-AIRS co-locations on which the scatter plot properties in Fig. 12 are based, are obtained by selecting the AIRS measurements with Qual_H2O flag equal to 0 or 1 with a maximum distance of 50 km between the ground pixel centre and the IGS station. As for the Brussels case study, we elaborate here more on these data criteria. We found that the sample of data with the best quality ($Qual_H2O = 0$) shows, in the (weighted) mean, higher maximum IWV values, a higher bias w.r.t. the coincident GPS IWV measurements, a lower RMS of the scatter plot, a higher correlation coefficient and a higher standard deviation of the regression slope coefficient. On the other hand, the mean IWV value and regression slope coefficient are nearly identical between both samples of different data quality. Of course, it should be mentioned that we compare two samples of different sizes: the sample of the highest data quality only has one eighth of the amount of observations of the sample with $Qual_H2O = 1$, which might have a significant impact on the scatter plots w.r.t. GPS. Alternatively, doubling the limiting distances between the AIRS ground pixel centres and the IGS stations leads, again in the mean, to a decrease of the bias (or a (more) negative bias), a higher RMS of the scatter plots, and lower correlation coefficients and regression slopes. These tendencies are in agreement with those found for the Brussels case study and were to be expected, although the absence of any impact of the Qual_H2O flag on the regression slope coefficient of the linear correlation with GPS is remarkable.

As AIRS has two overpasses a day above IGS stations with latitudes between $45^\circ N$ and $45^\circ S$, we can investigate the differences between daytime and nighttime IWV measurements for this satellite sounder. Observations with SZA lower than 90° are classified as daytime, for larger values of SZA, we speak about nighttime observations. We found that the AIRS nighttime measurements are consistently showing a better

the GPS, although this slope is still considerably lower than 1. We ascribe this to the fact that only radiosondes and GPS are all-weather devices, while the other three techniques demand an at least partly clear sky. Moreover, the GPS technique is known to be less sensitive for small amounts of IWV.

Comparing now the two satellite instruments, we conclude that both reveal a similar agreement w.r.t. GPS, although the AIRS instrument shows less variability in the scatter plot properties among the different selected stations. The largest difference between both comparisons with GPS IWVs is given by the regression slope coefficient: the mean slope of GOMESCIA considerably higher than the AIRS mean slope. This can partly be explained by the fact that for GOMESCIA, a small number of the stations have regression slopes superior to 1, while the maximum value for AIRS is about 0.95. The minimum slope coefficient for both techniques lies in the range 0.70 to 0.75. Moreover, it also seems that the AIRS slope coefficient is less sensitive to the selection of different samples of data with different fractions of cloud cover. Another possibility is that the AIRS cloud information flags are not very restrictive.

As for the Brussels station, we undertook subsequently an IWV techniques inter-comparison separately for the different seasons. A very similar seasonal behaviour of the different scatter plot properties for the different instruments is found for Brussels and the global (weighted) averages. Only during wintertime, the Brussels behaviour deviates from the global average for a small number of cases among all possible combinations of the scatter plot properties and instruments. As a result, we can confirm the identical seasonal dependence, for all instruments, of the globally averaged bias and RMS: the relative bias is minimal (or most negative) in summer (maximal mean IWV), and maximal in winter (minimal mean IWV), whereas the RMS is minimal in winter and maximal in summer. This latter finding for the RMS might be linked to the detected dependency of the RMS, also for all considered instruments, on latitude or mean IWV: the RMS w.r.t. GPS decreases with increasing latitude and decreasing mean IWV. Of course, in our sample there is a strong anti-correlation between the mean IWV and the latitude, so that this finding can be reduced to a strong correlation between RMS and

A multi-site IWV techniques intercomparison

R. Van Malderen et al.

[Title Page](#)[Abstract](#)[Introduction](#)[Conclusions](#)[References](#)[Tables](#)[Figures](#)[Back](#)[Close](#)[Full Screen / Esc](#)[Printer-friendly Version](#)[Interactive Discussion](#)

A multi-site IWV techniques intercomparison

R. Van Malderen et al.

Title Page

Abstract

Introduction

Conclusions

References

Tables

Figures

◀

▶

◀

▶

Back

Close

Full Screen / Esc

Printer-friendly Version

Interactive Discussion



IWV and an apparent anti-correlation between bias and IWV. The anti-correlation of the bias with GPS and mean IWV value can be easily explained by the fact that GPS instruments seem to have different sensitivities to IWV at the IWV extremes than the other instruments: for larger IWV values, which are more frequent in Northern Hemisphere (NH) summer season and at lower latitude stations, the GPS retrieval technique leads to higher IWV values than the other instruments, so that the IWV bias w.r.t. GPS (instrument minus GPS) will be smaller (or negative). The reverse reasoning can then be done for the lower end IWV values. Ohtani and Naito (2000) considered the effects of seasonal variation of the GPS mapping function as one of the causes for their observed annual variation of the GPS-RS biases. Indeed, the mapping function varies as the curvature of the atmosphere changes, which is determined basically by the changes in the ratio of the thickness of the atmosphere to the radius of the Earth. Hence, when the thickness changes according to the season, it results in the variation of the real mapping function. They found that the dependence of their GPS-RS bias could be reduced by tuning observed meteorological parameters like surface temperature, tropopause height, temperature lapse rate, and height of an isothermal layer in the mapping function. The tendency for the GPS-RS RMS to increase with IWV was also found and discussed by other authors (e.g. Deblonde et al., 2005, and references therein). They attributed this feature, in part to stronger humidity gradients that can exist between dry and moist air when moister air is involved. In the presence of strong gradients, the location and sampling differences between GPS and RS can be more significant than for lower IWV conditions. In addition, they claimed that the presence of strong horizontal gradients in atmospheric properties can have a negative impact on the ZTD accuracy due to a breakdown of the azimuthal symmetry assumption.

We end this section on the world-wide techniques intercomparison by making the consideration that we could not detect any clear dependency of the other scatter plot properties (bias, R^2 , and slope) on latitude, longitude, height and mean IWV of the IGS station for each of the techniques.

6 Conclusions

In this paper, we undertook a techniques intercomparison of different instruments measuring the total column water vapour in the troposphere. We first concentrated on Brussels, Belgium, as a case study. The main results for this mid-latitude site are summarized in Sect. 4.5 and might be directly compared to similar studies (see e.g. Schneider et al., 2010, for a subtropical site, and Buehler et al., 2012, for a subarctic location, and other references therein). Extending our methodology world-wide (i.e. to 28 NH stations, summary of the results is found in Sect. 5.5) and averaging, for each technique separately, the IWV differences (bias, RMS, R^2 , slope) with GPS over all the stations (with normalized weights the number of coincident pairs per station) revealed the same qualitative agreements with the co-located GPS station as for the Brussels case. Moreover, the conclusions drawn for the impact analysis of atmospheric conditions (clouds, night vs. day) and instrumental setups (satellite scan angle, distance between satellite ground pixel centre and station) on and the seasonal dependency of the techniques intercomparison are very similar for the global average and the Brussels case study. As a consequence, the Brussels station is really illustrative for the global NH average and represents an ideal location to demonstrate techniques intercomparison studies.

When going through the literature reports on similar techniques intercomparisons, it turns out that reported systematic differences between different instruments are study-dependent and show no overall consistent pattern. With this study, we attempted to characterize the systematic differences, besides the bias and RMS, also in terms of scatter plot properties like correlation coefficient and linear regression slope. We found that these characteristics are dependent on the individual instrument (not only the instrument type, as different CIMEL sun photometers compare differently with the same GPS at the same site) and on the location. But, on the other hand, no consistent overall picture emerges, as e.g. no clear geographical patterns could be detected for most of the characteristics, except for the RMS. Buehler et al. (2012) came to the same conclusion and made subsequently the consideration that it is therefore not obvious how the

A multi-site IWV techniques intercomparison

R. Van Malderen et al.

Title Page

Abstract

Introduction

Conclusions

References

Tables

Figures



Back

Close

Full Screen / Esc

Printer-friendly Version

Interactive Discussion



IWV measurement accuracy could be further improved and which technique is most suitable for recording climate data records from a scientific point of view.

Based on our study, we are less pessimistic and we argue that CIMEL sun photometers and GPS are very valuable techniques to measure IWV and the most promising to build up long time series for climate applications, as long as the data homogeneity can be guaranteed. For the CIMEL photometers belonging to the AERONET, a regular calibration of the instrument is required. GPS observations from the IGS network were (re)processed homogeneously from 1994 on to mid-April 2011 to provide ZTDs. Of course, the installation or the change of radomes and GPS antennas, elevation cut-off angle changes and changes in the observation statistics can introduce inhomogeneities in the station's ZTD time series (Vey et al., 2009). However, both instruments measure the water vapour content somewhat differently in either the driest or the wet regimes. For small IWV amounts, the GPS retrieval technique is less sensitive and underestimates the actual IWV amounts. For large IWV values, the GPS instrument measures higher amounts of IWV than the CIMEL – and the other instruments – do. This can at least partly be explained by the observation bias of the CIMEL instrument: it requires a clear sky in the direction of the sun. But the larger the IWV values, the higher the probability to have clouds, which contribute directly to the GPS IWVs, but not to the CIMEL IWVs. Also the different instrumental approaches to map the measurements in the zenith direction might contribute to the different sensitivity of the CIMEL and GPS devices to large and small amounts of IWV present in the atmosphere, as the comparison of coincident solar slant IWVs at Brussels showed. Also, Ohtani and Naito (2000) found that better tuning the seasonal variation of the mapping function used for the GPS IWV retrieval could reduce the GPS-RS dependence on IWV. To which extent these different sensitivities to the IWV extremes have an impact on trends, will be investigated in a forthcoming paper.

Satellite devices measuring in the visual and the thermal infrared the IWV are susceptible to a similar observation bias as the CIMEL (for low cloud fractions only), which is also reflected in the low mean value of the regression line slope. For these satellite

A multi-site IWV techniques intercomparison

R. Van Malderen et al.

Title Page

Abstract

Introduction

Conclusions

References

Tables

Figures



Back

Close

Full Screen / Esc

Printer-friendly Version

Interactive Discussion



A multi-site IWV techniques intercomparison

R. Van Malderen et al.

Title Page

Abstract

Introduction

Conclusions

References

Tables

Figures

◀

▶

◀

▶

Back

Close

Full Screen / Esc

Printer-friendly Version

Interactive Discussion



data, the largest geographical variability of the IWV measurements relative to the co-located GPS observations is obtained, possibly due to the spatial coverage and the high variance of IWV. From the comparison of the GOMESCIA measurements with the 28 co-located GPS stations, it seems feasible to build up a time series of IWV values retrieved by those three different instruments. In a forthcoming paper, we will compare the resulting GOMESCIA IWV trends for more than 15 yr with the trends calculated from IWV values retrieved at co-located GPS stations in order to investigate the impact of the GOMESCIA clear sky observation bias and to identify jumps due to the change from one satellite instrument to another.

Acknowledgements. This research was initiated under the AGACC project (contract SD/AT/01A) and continued in the framework of the Solar-Terrestrial Centre of Excellence (STCE), both funded by the Belgian Federal Science Policy Office. The authors are grateful to all colleagues and data providers having participated in this study, in particular K. Mies (MPI-C), who contributed substantially to the technical development of the GOMESCIA IWV retrieval algorithm. We also want to thank the PIs and operators of all instruments whose data have been used in this paper. We are also indebted to the IGS and the AERONET for their excellent network management, making such research possible. The CIMEL Calibration of a range of CIMEL instruments used in this research was performed at the AERONET-EUROPE calibration centre, supported by ACTRIS (European Union Seventh Framework Program FP7/2007-2013 under grant agreement no. 262254).

References

- Alexandrov, M. D., Schmid, B., Turner, D. D., Cairns, B., Oinas, V., Lacis, A. A., Gutman, S. I., Westwater, E. R., Smirnov, A., and Eilers, J.: Columnar water vapor retrievals from multifilter rotating shadowband radiometer data, *J. Geophys. Res.*, 114, D02306, doi:10.1029/2008JD010543, 2009.
- Askne, J. and Nordius, H.: Estimation of tropospheric delay for microwaves from surface weather data, *Radio Sci.*, 22, 379–386, 1987.
- Aumann, H. H., Chahine, M. T., Gautier, C., Goldberg, M. D., Kalnay, E., McMillin, L. M., Revercomb, H., Rosenkranz, P. W., Smith, W. L., Staelin, D. H., Strow, L. L., and Susskind, J.:

A multi-site IWV techniques intercomparison

R. Van Malderen et al.

Title Page

Abstract

Introduction

Conclusions

References

Tables

Figures

◀

▶

◀

▶

Back

Close

Full Screen / Esc

Printer-friendly Version

Interactive Discussion



AIRS/AMSU/HSB on the Aqua mission: design, science objectives, data products, and processing systems, *IEEE T. Geosci. Remote*, 41, 253–264, doi:10.1109/TGRS.2002.808356, 2003.

5 Bedka, S., Knuteson, R., Revercomb, H., Tobin, D., and Turner, D.: An assessment of the absolute accuracy of the Atmospheric Infrared Sounder v5 precipitable water vapor product at tropical, midlatitude, and arctic ground-truth sites: September 2002 through August 2008, *J. Geophys. Res.*, 115, D17310, doi:10.1029/2009JD013139, 2010.

10 Bevis, M., Businger, S., Herring, T. A., Rocken, C., Anthes, R. A., and Ware, R. H.: GPS meteorology: remote sensing of atmospheric water vapor using the global positioning system, *J. Geophys. Res.*, 97, 15787–15801, doi:10.1029/92JD01517, 1992.

Bevis, M., Businger, S., Chiswell, S., Herring, T. A., Anthes, R. A., Rocken, C., and Ware, R. H.: GPS meteorology: mapping zenith wet delays onto precipitable water, *J. Appl. Meteorol.*, 33, 379–386, doi:10.1175/1520-0450(1994)033<0379:GMMZWD>2.0.CO;2, 1994.

15 Bock, O., Bouin, M.-N., Walpersdorf, A., Lafore, J. P., Janicot, S., Guichard, F., and Agustí-Panareda, A.: Comparison of groundbased GPS precipitable water vapour to independent observations and NWP model reanalyses over Africa, *Q. J. Roy. Meteor. Soc.*, 133, 2011–2027, doi:10.1002/qj.185, 2007.

20 Boehm, J., Niell, A., Tregoning, P., and Schuh, H.: Global Mapping Function (GMF): a new empirical mapping function based on numerical weather model data, *Geophys. Res. Lett.*, 33, L07304, doi:10.1029/2005GL025546, 2006.

Brenot, H., Ducrocq, V., Walpersdorf, A., Champollion, C., and Caumont, O.: GPS zenith delay sensitivity evaluated from high-resolution numerical weather prediction simulations of the 8–9 September 2002 flash flood over southeastern France, *J. Geophys. Res.*, 111, D15105, doi:10.1029/2004JD005726, 2006.

25 Bruegge, C. J., Conel, J. E., Green, R. O., Margolis, J. S., Holm, R. G., and Toon, G.: Water vapor column abundances retrievals during FIFE, *J. Geophys. Res.*, 97, 18759–18768, doi:10.1029/92JD01050, 1992.

Buehler, S. A., Östman, S., Melsheimer, C., Holl, G., Eliasson, S., John, V. O., Blumenstock, T., Hase, F., Elgered, G., Raffalski, U., Nasuno, T., Satoh, M., Milz, M., and Mendrok, J.: A multi-instrument comparison of integrated water vapour measurements at a high latitude site, *Atmos. Chem. Phys.*, 12, 10925–10943, doi:10.5194/acp-12-10925-2012, 2012.

30 Businger, S., Chiswell, S. R., Bevis, M., Duan, J., Anthes, R. A., Rocken, C., Ware, R. H., Exner, M., Van Hove, T., and Solheim, F. S.: The promise of

A multi-site IWV techniques intercomparison

R. Van Malderen et al.

Title Page

Abstract

Introduction

Conclusions

References

Tables

Figures

◀

▶

◀

▶

Back

Close

Full Screen / Esc

Printer-friendly Version

Interactive Discussion



GPS in atmospheric monitoring, *B. Am. Meteorol. Soc.*, 77, 5–18, doi:10.1175/1520-0477(1996)077<0005:TPOGIA>2.0.CO;2, 1996.

Byun, S. H. and Bar-Sever, Y. E.: A new type of troposphere zenith path delay product of the international GNSS service, *J. Geodesy*, 83, 367–373, doi:10.1007/s00190-008-0288-8, 2009.

Byun, S. H. and Bar-Sever, Y. E.: The Re-Analysis of the IGS Tropospheric Product, IGS workshop, Newcastle, 28 June–1 July 2010, available at: http://acc.igs.org/tropo/tropo-repro_IGSW10.pdf (last access: 15 February 2012), 2010.

Chen, G. and Herring, T. A.: Effects of atmospheric azimuthal asymmetry on the analysis of space geodetic data, *J. Geophys. Res.*, 102, 20489–20502, doi:10.1029/97JB01739, 1997.

Dai, A., Wang, J., Thorne, P. W., Parker, D. E., Haimberger, L., and Wang, X. L.: A new approach to homogenize daily radiosonde humidity data, *J. Climate*, 24, 965–991, doi:10.1175/2010JCLI3816.1, 2011.

Davis, J. L., Herring, T. A., Shapiro, I. I., Rogers, A. E. E., and Elgered, G.: Geodesy by interferometry: effects of atmospheric modeling errors on estimates of baseline length, *Radio Sci.*, 20, 1593–1607, 1985.

Deblonde, G., Macpherson, S., Mireault, Y., and Heroux, P.: Evaluation of GPS precipitable water over Canada and the IGS network, *J. Appl. Meteorol.*, 44, 153–166, doi:10.1175/JAM-2201.1, 2005.

De Bock, V., De Backer, H., Mangold, A., and Delcloo, A.: Aerosol Optical Depth measurements at 340 nm with a Brewer spectrophotometer and comparison with Cimel sunphotometer observations at Uccle, Belgium, *Atmos. Meas. Tech.*, 3, 1577–1588, doi:10.5194/amt-3-1577-2010, 2010.

Dow, J. M., Neilan, R. E., and Rizos, C.: The international GNSS service in a changing landscape of global navigation satellite systems, *J. Geodesy*, 83, 191–198, doi:10.1007/s00190-008-0300-3, 2009.

Duan, J., Bevis, M., Fang, P., Bock, Y., Chiswell, S., Businger, S., Rocken, C., Solheim, F., Van Hove, T., Ware, R., McClusky, S., Herring, T. A., and King, R. W.: GPS meteorology: direct estimation of the absolute value of precipitable water, *J. Appl. Meteorol.*, 35, 830–838, doi:10.1175/1520-0450(1996)035<0830:GMDEOT>2.0.CO;2, 1996.

Durre, I., Vose, R. S., and Wuertz, D. B.: Overview of the integrated global radiosonde archive, *J. Climate*, 19, 53–68, doi:10.1175/JCLI3594.1, 2006.

A multi-site IWV techniques intercomparison

R. Van Malderen et al.

Title Page

Abstract

Introduction

Conclusions

References

Tables

Figures

◀

▶

◀

▶

Back

Close

Full Screen / Esc

Printer-friendly Version

Interactive Discussion



Durre, I., Junior, C. N. W., Yin, X., and Vose, R. S.: Radiosonde-based trends in precipitable water over the Northern Hemisphere: an update, *J. Geophys. Res.*, 114, D05112, doi:10.1029/2008JD010989, 2009.

Elgered, G., Davis, J. L., Herring, T. A., and Shapiro, I. I.: Geodesy by radio interferometry: water vapour radiometry for estimation of the wet delay, *J. Geophys. Res.*, 96, 6541–6555, doi:10.1029/90JB00834, 1991.

EUMETSAT: Algorithm Theoretical Basis Document for GOME-2 Total Column Products of Ozone, NO₂, tropospheric NO₂, BrO, SO₂, H₂O, HCHO, OCIO and Cloud Properties (GDP 4.4 for O3M-SAF OTO and NTO), available at: http://atmos.caf.dlr.de/gome2/docs/DLR_GOME-2_ATBD.pdf (last access: 28 April 2013), 2010.

Fetzer, E., McMillin, L. M., Tobin, D., Aumann, H. H., Gunson, M. R., McMillan, W. W., Hagan, D. E., Hofstadter, M. D., Yoe, J., Whiteman, D. N., Barnes, J. E., Bennartz, R., Vomel, H., Walden, V., Newchurch, M., Minnett, P. J., Atlas, R., Schmidlin, F., Olsen, E. T., Goldberg, M. D., Sisong, Z., HanJung, D., Smith, W. L., and Revercomb, H.: AIRS/AMSU/HSB validation, *IEEE T. Geosci. Remote*, 41, 418–431, doi:10.1109/TGRS.2002.808293, 2003.

Fetzer, E. J., Eldering, A., and Lee, S.-Y.: Characterization of AIRS temperature and water vapor measurement capability using correlative observations, paper presented at the 85th Annual Meeting of the Am. Meteorol. Soc., San Diego, California, 9–13 January 2005, available at: <http://ams.confex.com/ams/pdfpapers/86552.pdf> (last access: 21 March 2013), 2005.

Fetzer, E. J., Lambrigtsen, B. H., Eldering, A., Aumann, H. H., and Chahine, M. T.: Biases in total precipitable water vapor climatologies from atmospheric infrared sounder and advanced microwave scanning radiometer, *J. Geophys. Res.*, 111, D09S16, doi:10.1029/2005JD006598, 2006.

Gaffen, D. J. and Elliott, W. P.: Column water vapor content in clear and cloudy skies, *J. Climate*, 6, 2278–2287, doi:10.1175/1520-0442(1993)006<2278:CWVCIC>2.0.CO;2, 1993.

Gutman, S. I., Sahm, S., Stewart, J., Benjamin, S., Smith, T., and Schwartz, B.: A new composite observing system strategy for ground-based GPS meteorology, paper presented at the 12th Symposium on Meteorological Observations and Instrumentation, Am. Meteorol. Soc., Boston, 9–13 February 2003, available at: <https://ams.confex.com/ams/pdfpapers/54168.pdf> (last access: 20 June 2012), 2003.

Hagemann, S., Bengtsson, L., and Gendt, G.: On the determination of atmospheric water vapor from GPS measurements, *J. Geophys. Res.*, 108, 4678, doi:10.1029/2002JD003235, 2003.

A multi-site IWV techniques intercomparison

R. Van Malderen et al.

Title Page

Abstract

Introduction

Conclusions

References

Tables

Figures

◀

▶

◀

▶

Back

Close

Full Screen / Esc

Printer-friendly Version

Interactive Discussion



- IGS ACC Website: IGS data reprocessing campaign: REPRO1, available at: <http://acc.igs.org/reprocess.html> (last access: 18 March), 2013.
- Hocke, K. and Martine, L.: Survey of inter-comparisons of water vapour measurements, in: *Monitoring Atmospheric Water Vapour*, ISSI Scientific Report Series, 10, edited by: Kämpfer, N., 10, 243–288, doi:10.1007/978-1-4614-3909-7_11, 2013.
- Hogg, D. C., Guiraud, F. O., and Decker, M. T.: Measurement of excess transmission length on Earth–space paths, *Astron. Astrophys.*, 95, 304–307, 1981.
- Holben, B. N., Eck, T. F., Slutsker, I., Smirnov, A., Sinyuk, A., Schafer, J., Giles, D., and Dubovik, O.: AERONET's Version 2.0 quality assurance criteria, in: *Proc. SPIE 6408, Remote Sensing of the Atmosphere and Clouds, 64080Q*, 28 November 2006, doi:10.1117/12.706524, 2006.
- Kämpfer, N.: *Monitoring Atmospheric Water Vapour*, ISSI Scientific Report Series, 10, 175–214, doi:10.1007/978-1-4614-3909-7_9, 2013.
- Kasten, F. and Young, A. T.: Revised optical air mass tables and approximation formula, *Appl. Optics*, 28, 4735–4738, 1989.
- Kuo, Y.-H., Guo, Y.-R., and Westwater, E. R.: Assimilation of precipitable water measurements into a mesoscale numerical model, *Mon. Weather Rev.*, 121, 1215–1238, doi:10.1175/1520-0493(1993)121<1215:AOPWMI>2.0.CO;2, 1993.
- Leiterer, U., Dier, H., Nagel, D., Naebert, T., Althausen, D., Franke, K., Kats, A., and Wagner, F.: Correction method for RS80-A Humicap humidity profiles and their validation by lidar backscattering profiles in tropical cirrus clouds, *J. Atmos. Ocean. Tech.*, 22, 18–29, doi:10.1175/JTECH-1684.1, 2005.
- Mattar, C., Sobrino, J. A., Julien, Y., and Morales, L.: Trends in column integrated water vapour over Europe from 1973 to 2003, *Int. J. Climatol.*, 31, 1749–1757, doi:10.1002/joc.2186, 2011.
- McCarthy, M. P., Thorne, P. W., and Titchner, H. A.: An analysis of tropospheric humidity trends from radiosondes, *J. Climate*, 22, 5820–5838, doi:10.1175/2009JCLI2879.1, 2009.
- Mears, C. A., Santer, B. D., Wentz, F. J., Taylor, K. E., and Wehner, M. F.: Relationship between temperature and precipitable water changes over tropical oceans, *Geophys. Res. Lett.*, 34, L24709, doi:10.1029/2007GL031936, 2007.
- Mieruch, S., Schröder, M., Noël, S., and Schulz, J.: Comparison of monthly means of global total column water vapor retrieved from independent satellite observations, *J. Geophys. Res.*, 115, D23310, doi:10.1029/2010JD013946, 2010.

A multi-site IWV techniques intercomparison

R. Van Malderen et al.

Title Page

Abstract

Introduction

Conclusions

References

Tables

Figures

◀

▶

◀

▶

Back

Close

Full Screen / Esc

Printer-friendly Version

Interactive Discussion



Miloshevich, L. M., Vömel, H., Whiteman, D. N., and Leblanc, T.: Accuracy assessment and correction of Vaisala RS92 radiosonde water vapor measurements, *J. Geophys. Res.*, 114, D11305, doi:10.1029/2008JD011565, 2009.

Noël, S., Mieruch, S., Bovensmann, H., and Burrows, J. P.: Preliminary results of GOME-2 water vapour retrievals and first applications in polar regions, *Atmos. Chem. Phys.*, 8, 1519–1529, doi:10.5194/acp-8-1519-2008, 2008.

Ohtani, R. and Naito, I.: Comparisons of GPS-derived precipitable water vapors with radiosonde observations in Japan, *J. Geophys. Res.*, 105, 26917–26929, doi:10.1029/2000JD900362, 2000.

Palm, M., Melsheimer, C., Noël, S., Heise, S., Notholt, J., Burrows, J., and Schrems, O.: Integrated water vapor above Ny Ålesund, Spitsbergen: a multi-sensor intercomparison, *Atmos. Chem. Phys.*, 10, 1215–1226, doi:10.5194/acp-10-1215-2010, 2010.

Raja, M. K. R. V., Gutman, S. I., Yoe, J. G., McMillin, L. M., and Zhao, J.: The validation of AIRS retrievals of integrated precipitable water vapor using measurements from a network of ground-based GPS receivers over the contiguous United States, *J. Atmos. Ocean. Tech.*, 25, 416–428, doi:10.1175/2007JTECHA889.1, 2008.

Ray, J.: [IGSMail-6475] Use of IGS orbits for homogeneous long-term processing, available at: <http://igs.cb.jpl.nasa.gov/pipermail/igsmail/2011/006467.html> (last access: 31 January 2012), 2011.

Reischung, P., Griffiths, J., Ray, J., Schmid, R., Collilieux, X., and Garayt, B.: IGS08: the IGS realization of ITRF2008, *GPS Solut.*, 16, 483–494, doi:10.1007/s10291-011-0248-2, 2012.

Ross, R. J. and Elliott, W. P.: Radiosonde-based Northern Hemisphere tropospheric water vapor trends, *J. Climate*, 14, 1602–1612, doi:10.1175/1520-0442(2001)014<1602:RBNHTW>2.0.CO;2, 2001.

Rocken, C., Ware, R., Van Hove, T., Solheim, F., Alber, C., Johnson, J., Bevis, M., and Businger, S.: Sensing atmospheric water vapor with the global positioning system, *Geophys. Res. Lett.*, 20, 2631–2634, doi:10.1029/93GL02935, 1993.

Rocken, C., Van Hove, T., Johnson, J., Solheim, F., Ware, R., Bevis, M., Chiswell, S., and Businger, S.: GPS/STORM–GPS sensing of atmospheric water vapor for meteorology, *J. Atmos. Ocean. Tech.*, 12, 468–478, doi:10.1175/1520-0426(1995)012<0468:GSOAWV>2.0.CO;2, 1995.

Saastamoinen, J.: Atmospheric correction for the troposphere and stratosphere in radio ranging of satellites, in: *The Use of Artificial Satellites for Geodesy*, *Geophys. Monogr. Ser.*, 15, edited

A multi-site IWV techniques intercomparison

R. Van Malderen et al.

Title Page

Abstract

Introduction

Conclusions

References

Tables

Figures

◀

▶

◀

▶

Back

Close

Full Screen / Esc

Printer-friendly Version

Interactive Discussion



by: Henriksen, S. W., Mancini, A., and Chovitz, B. H., AGU, Washington, D.C., 247–251, 1972.

Schmid, B., Michalsky, J. J., Slater, D. W., Barnard, J. C., Halthore, R. N., Liljegren, J. C., Holben, B. N., Eck, T. F., Livingston, J. M., Russell, P. B., Ingold, T., and Slutsker, I.: Comparison of columnar water-vapor measurements from solar transmittance methods, *Appl. Optics*, 40, 1886–1896, 2001.

Schmid, R.: [IGSMail-6355] Upcoming switch to IGS08/igs08.atx – Details on igs08.atx, available at: <http://igscb.jpl.nasa.gov/pipermail/igsmail/2011/006347> (last access: 15 February 2012), 2011.

Schneider, M., Romero, P. M., Hase, F., Blumenstock, T., Cuevas, E., and Ramos, R.: Continuous quality assessment of atmospheric water vapour measurement techniques: FTIR, Cimel, MFRSR, GPS, and Vaisala RS92, *Atmos. Meas. Tech.*, 3, 323–338, doi:10.5194/amt-3-323-2010, 2010.

Schröder, M. and Bojkov, B.: GLOBVAPOR, Project Validation Report (PVR) of GOME+SCIAMACHY+GOME-2, ESRIN/AO/1-6090/09/I-OL Version 3.0, available at: http://www.globvapour.info/download/GlobVapour_D19_PVR_GOME_SCIAMACHY_V3.0.pdf (last access: 28 April 2013), 2012.

Smit, H., Kivi, R., Vömel, H., and Paukkunen, A.: Thin film capacitive sensors, in: *Monitoring Atmospheric Water Vapour*, ISSI Scientific Report Series, edited by: Kämpfer, N., 10, 11–38, doi:10.1007/978-1-4614-3909-7_2, 2013.

Soden, B. J. and Held, I. M.: An assessment of climate feedbacks in coupled ocean–atmosphere models, *J. Climate*, 19, 3354–3360, doi:10.1175/JCLI3799.1, 2006.

Suortti, T. M., Kivi, R., Kats, A., Yushkov, V., Kämpfer, N., Leiterer, U., Miloshevich, L. M., Neuber, R., Paukkunen, A., Ruppert, P., and Vömel, H.: Tropospheric comparisons of Vaisala radiosondes and Balloon–Borne frost-point and Lyman- α hygrometers during the LAUTLOS-WAVVAP experiment, *J. Atmos. Ocean. Tech.*, 25, 149–166, doi:10.1175/2007JTECHA887.1, 2008.

Tregoning, P., Boers, R., O'Brien, D., and Hendy, M.: Accuracy of absolute precipitable water vapor estimates from GPS observations, *J. Geophys. Res.*, 103, 28701–28710, doi:10.1029/98JD02516, 1998.

Trenberth, K. E., Fasullo, J., and Smith, L.: Trends and variability in column-integrated atmospheric water vapor, *Clim. Dynam.*, 24, 741–758, doi:10.1007/s00382-005-0017-4, 2005.

A multi-site IWV techniques intercomparison

R. Van Malderen et al.

Title Page

Abstract

Introduction

Conclusions

References

Tables

Figures

◀

▶

◀

▶

Back

Close

Full Screen / Esc

Printer-friendly Version

Interactive Discussion



Urban, J.: Satellite sensors measuring atmospheric water vapour, in: Monitoring Atmospheric Water Vapour, ISSI Scientific Report Series, edited by: Kämpfer, N., 10, 175–214, doi:10.1007/978-1-4614-3909-7_9, 2013.

Van Malderen, R. and De Backer, H.: A drop in upper tropospheric humidity in autumn 2001, as derived from radiosonde measurements at Uccle, Belgium, *J. Geophys. Res.*, 115, D20114, doi:10.1029/2009JD013587, 2010.

Vey, S., Dietrich, R., Fritsche, M., Rülke, A., Steigenberger, P., and Rothacher, M.: On the homogeneity and interpretation of precipitable water time series derived from global GPS observations, *J. Geophys. Res.*, 114, D10101, doi:10.1029/2008JD010415, 2009.

Vey, S., Dietrich, R., Rülke, A., Fritsche, M., Steigenberger, P., and Rothacher, M.: Validation of precipitable water vapor within the NCEP/DOE reanalysis using global GPS observations from one decade, *J. Climate*, 23, 1675–1695, doi:10.1175/2009JCLI2787.1, 2010.

Vömel, K., Selkirk, H., Miloshevich, L., Valverde-Canossa, J., Valdés, J., Kyrö, E., Kivi, R., Stolz, W., Peng, G., and Diaz, J. A.: Radiation dry bias of the Vaisala RS92 humidity sensor, *J. Atmos. Ocean. Tech.*, 24, 953–963, doi:10.1175/JTECH2019.1, 2007.

Wagner, T., Beirle, S., Grzegorski, M., and Platt, U.: Global trends (1996–2003) of total column precipitable water observed by Global Ozone Monitoring Experiment (GOME) on ERS-2 and their relation to near-surface temperature, *J. Geophys. Res.*, 111, D12102, doi:10.1029/2005JD006523, 2006.

Wagner, T., Beirle, S., and Mies, K.: Description of the MPI-Mainz H₂O retrieval (Version 5.0, March 2011), http://www.sciamachy.org/products/H2O/H2Ovc_IUP_AD.pdf (last access: 4 April 2013), 2011.

Wagner, T., Andreae, M. O., Beirle, S., Dörner, S., Mies, K., and Shaiganfar, R.: MAX-DOAS observations of the total atmospheric water vapour column and comparison with independent observations, *Atmos. Meas. Tech.*, 6, 131–149, doi:10.5194/amt-6-131-2013, 2013.

Wang, J. and Zhang, L.: Systematic errors in global radiosonde precipitable water data from comparisons with groundbased GPS measurements, *J. Climate*, 21, 2218–2238, doi:10.1175/2007JCLI1944.1, 2008.

Wang, J., Zhang, L., and Dai, A.: Global estimates of water-vapor-weighted mean temperature of the atmosphere for GPS applications, *J. Geophys. Res.*, 110, D21101, doi:10.1029/2005JD006215, 2005.

A multi-site IWV techniques intercomparison

R. Van Malderen et al.

Title Page

Abstract

Introduction

Conclusions

References

Tables

Figures

◀

▶

◀

▶

Back

Close

Full Screen / Esc

Printer-friendly Version

Interactive Discussion



Wang, J., Zhang, L., Dai, A., Van Hove, T., and Van Baelen, J.: A near-global, 2 hourly data set of atmospheric precipitable water from ground-based GPS measurements, *J. Geophys. Res.*, 112, D11107, doi:10.1029/2006JD007529, 2007.

Wang, J., Zhang, L., Dai, A., Immler, F., Sommer, M., and Vömel, H.: Radiation dry bias correction of Vaisala RS92 humidity data and its impacts on historical radiosonde data, *J. Atmos. Ocean. Tech.*, 30, 197–214, doi:10.1175/JTECH-D-12-00113.1, 2013.

Ware, R., Alber, C., Rocken, C., and Solheim, F.: Sensing integrated water vapor along GPS ray paths, *Geophys. Res. Lett.*, 24, 417–420, 1997.

Wentz, F. J., Ricciardulli, L., Hilburn, K., and Mears, C.: How much more rain will global warming bring?, *Science*, 317, 233–235, doi:10.1126/science.1140746, 2007.

Zhao, T., Dai, A., and Wang, J.: Trends in tropospheric humidity from 1970 to 2008 over China from a homogenized radiosonde dataset, *J. Climate*, 25, 4549–4567, doi:10.1175/JCLI-D-11-00557.1, 2012.

Zumberge, J. F., Heflin, M. B., Jefferson, D. C., Watkins, M. M., and Webb, F. H.: Precise point positioning for the efficient and robust analysis of GPS data from large networks, *J. Geophys. Res.*, 102, 5005–5017, doi:10.1029/96JB03860, 1997.

A multi-site IWV techniques intercomparison

R. Van Malderen et al.

Title Page

Abstract

Introduction

Conclusions

References

Tables

Figures

◀

▶

◀

▶

Back

Close

Full Screen / Esc

Printer-friendly Version

Interactive Discussion



Table 1. Main characteristics of the different techniques used.

	GPS	RS	CIMEL	GOMESCIA	AIRS
spatial coverage	±350 active IGS stations	±1500 IGRA sites	±300 AERONET sites	global	global
spatial resolution	cone, representative for about 100 km ²	point, horizontal displacement depending on the wind	point, horizontal displacement depending on SZA	GOME: 40 km × 320 km, SCIAMACHY: 30 km × 60 km, GOME-2: 40 km × 80 km	ellipsoidal, with major axis varying from 13.5 km (at nadir) to 31.5 km
temporal resolution	every 5 min	on average twice/day	±15 min, depending on weather conditions	GOME, SCIAMACHY: max. once/day; GOME-2: max. twice/day ^a	maximum twice/day
temporal coverage	1995–now	1950s–now	1993–now	1996–now	2002–now
All weather?	yes	yes	Clear sky	only if (almost) cloud free	only if (almost) cloud free
All direction	yes	vertical profile	solar direction	nadir	nadir/limb
Precision	< 2 mm ^b	≈ 5% (≈ 15% for very dry conditions) ^c	≈ 10% ^d	≈ 15% for clear sky ^e	≈ 5% ^f

^a for high latitudes, the broad swath orbits from GOME-2 overlap, i.e. for GOME-2 there can be 2 overpasses per day with a time difference of about 1.5 h.

^b Deblonde et al., 2005; Wang et al., 2007; Vey et al., 2010.

^c Miloshevich et al., 2009; Smit et al., 2012; Wang et al., 2013.

^d Alexandrov et al., 2009.

^e EUMETSAT, 2010.

^f Fetzer et al., 2003.

A multi-site IWV techniques intercomparison

R. Van Malderen et al.

Table 2. Scatter plot properties for the different IWV measurements, calculated for the IGS station FFMJ with surface observations from different WMO SYNOP stations. The reference WMO station has code 10637, also shown are the altitude and the height and horizontal distance from the IGS station FFMJ.

WMO	h [m]	Δh [m]	Δd [km]	N	bias	RMS	R^2	slope	offset
10532	205	74	36	62 348	0.08	0.32	0.999	1.002	0.051
10635	826	696	29	44 673	1.41	0.30	0.999	0.996	1.476
10637	113	−17	24						

[Title Page](#)
[Abstract](#)
[Introduction](#)
[Conclusions](#)
[References](#)
[Tables](#)
[Figures](#)
[⏪](#)
[⏩](#)
[◀](#)
[▶](#)
[Back](#)
[Close](#)
[Full Screen / Esc](#)
[Printer-friendly Version](#)
[Interactive Discussion](#)


A multi-site IWV techniques intercomparison

R. Van Malderen et al.

Title Page

Abstract

Introduction

Conclusions

References

Tables

Figures

◀

▶

◀

▶

Back

Close

Full Screen / Esc

Printer-friendly Version

Interactive Discussion



Table 3. Scatter plot properties for the different IWV measurements, calculated for the IGS station FFMJ with surface observations from different WMO SYNOP stations at one hand, and the co-located CIMEL sun photometer at the other hand.

<i>WMO</i>	<i>N</i>	bias	RMS	R^2	slope	offset
10532	3624	−0.51	1.48	0.984	0.887	1.134
10635	2965	−2.26	1.40	0.986	0.896	−0.557
10637	3614	−0.57	1.42	0.985	0.894	0.993

Table 4. List of the selected IGS stations, with latitude, longitude and altitude and the used WMO meteorological station to convert the ZTD to IWV. The latter 3 columns represent the WMO station height and the vertical and horizontal distances between the IGS and WMO station.

<i>IGS</i>	lat	lon	alt [m]	<i>WMO</i>	alt [m]	Δz [m]	Δd [km]
<i>BDOS</i>	13.09	-59.61	9.19	<i>78954</i>	56.00	46.81	35.01
<i>GUUG</i>	13.43	144.80	79.83	<i>91212</i>	75.30	-4.53	39.83
<i>AOML</i>	25.73	-80.16	27.43	<i>72202</i>	5.00	-22.43	32.27
<i>BRMU</i>	32.37	-64.70	20.83	<i>78016</i>	130.00	109.17	32.51
<i>SUWN</i>	37.28	127.05	58.81	<i>47101</i>	78.71	19.90	45.04
<i>GODE</i>	39.02	-76.83	47.77	<i>72405</i>	20.00	-27.77	42.00
<i>ANKR</i>	39.89	32.76	938.82	<i>17128</i>	959.00	20.18	28.92
<i>NISU</i>	40.00	-105.26	1669.72	<i>72476</i>	1473.00	-196.72	37.32
<i>MARS</i>	43.28	5.35	12.26	<i>7650</i>	32.00	19.74	18.29
<i>TLSE</i>	43.56	1.48	157.73	<i>7630</i>	158.00	0.27	29.91
<i>BUCU</i>	44.46	26.13	107.67	<i>15420</i>	91.00	-16.67	19.46
<i>HLFX</i>	44.68	-63.61	24.48	<i>71395</i>	145.40	120.93	29.38
<i>VENE</i>	45.44	12.33	23.20	<i>16098</i>	42.00	18.80	21.49
<i>OBE2</i>	48.09	11.28	595.22	<i>10865</i>	525.60	-69.62	1.86
<i>OPMT</i>	48.84	2.33	77.96	<i>7149</i>	90.00	12.04	45.79
<i>FFMJ</i>	50.09	8.67	130.17	<i>10637</i>	113.00	-17.17	23.88
<i>GLSV</i>	50.36	30.50	200.77	<i>33345</i>	167.00	-33.77	17.76
<i>BRUS</i>	50.80	4.36	104.22	<i>6447</i>	101.00	-3.22	0.20
<i>LEIJ</i>	51.35	12.37	134.22	<i>10469</i>	135.50	1.28	19.39
<i>PICL</i>	51.48	-90.16	353.08	<i>71845</i>	386.20	33.12	24.63
<i>DLFT</i>	51.99	4.39	30.59	<i>6210</i>	1.38	-29.21	15.81
<i>KSTU</i>	55.99	92.79	249.09	<i>29570</i>	276.15	27.06	21.47
<i>CHUR</i>	58.76	-94.09	28.80	<i>71913</i>	29.26	0.46	29.26
<i>SCOR</i>	70.49	-21.95	71.67	<i>4339</i>	71.46	-0.21	26.04
<i>TIXI</i>	71.63	128.87	53.91	<i>21824</i>	7.00	-46.91	33.66
<i>RESO</i>	74.69	-94.89	28.00	<i>71924</i>	67.68	39.68	30.56
<i>THU1</i>	76.54	-68.79	38.63	<i>4202</i>	59.00	20.37	25.83
<i>NYA1</i>	78.93	11.87	48.65	<i>1007</i>	7.70	-40.95	42.93

A multi-site IWV techniques intercomparison

R. Van Malderen et al.

Title Page

Abstract Introduction

Conclusions References

Tables Figures

◀ ▶

◀ ▶

Back Close

Full Screen / Esc

Printer-friendly Version

Interactive Discussion



A multi-site IWV techniques intercomparison

R. Van Malderen et al.

Table 5. Summary of the scatter plot properties of the IWV retrievals for different techniques w.r.t. the coincident GPS IWV retrievals for the case study of the Brussels site.

	N	bias	RMS	R^2	slope
CIMEL	9452	0.16	0.96	0.993	0.913
RS	3031	0.51	1.53	0.979	0.969
RS80	1531	0.41	1.80	0.970	0.955
RS9x	1500	0.61	1.18	0.988	0.984
GOMESCIA	2168	-0.51	3.71	0.866	0.825
GOME	918	-0.47	3.67	0.871	0.812
SCIAMACHY	379	-0.64	3.49	0.876	0.868
GOME-2	871	-0.49	3.86	0.855	0.822
AIRS	4461	0.01	3.51	0.883	0.842

Title Page

Abstract

Introduction

Conclusions

References

Tables

Figures

◀

▶

◀

▶

Back

Close

Full Screen / Esc

Printer-friendly Version

Interactive Discussion



**A multi-site IWV
techniques
intercomparison**

R. Van Malderen et al.

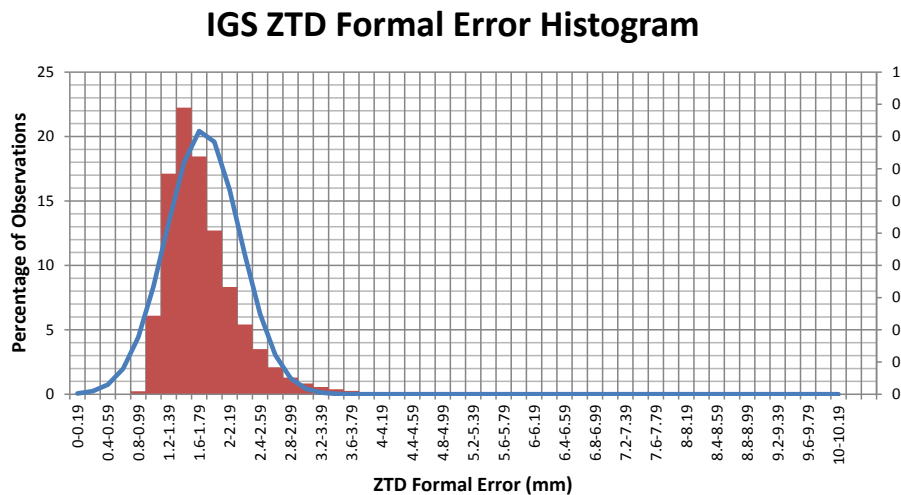


Fig. 1. Histogram of the formal error of the IGS troposphere product (over the complete IGS network and the complete 15+ yr history).

[Title Page](#)[Abstract](#)[Introduction](#)[Conclusions](#)[References](#)[Tables](#)[Figures](#)[⏪](#)[⏩](#)[◀](#)[▶](#)[Back](#)[Close](#)[Full Screen / Esc](#)[Printer-friendly Version](#)[Interactive Discussion](#)

AMTD

7, 1075–1151, 2014

A multi-site IWV techniques intercomparison

R. Van Malderen et al.

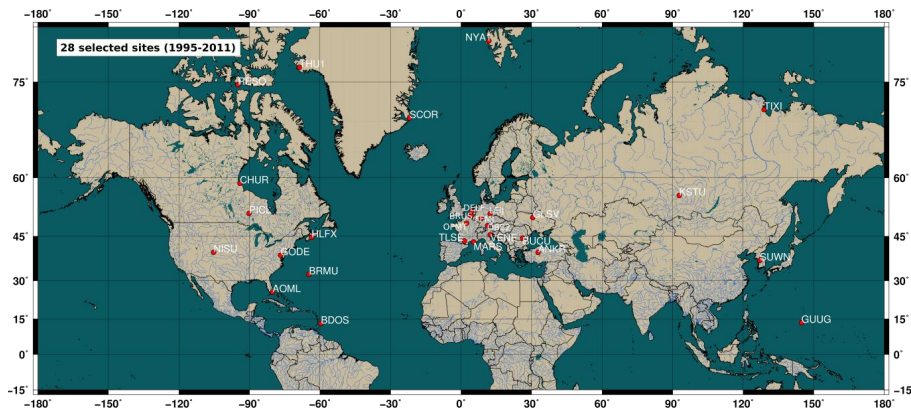


Fig. 2. Map of the selected sites that host at least 2 of the considered ground-based or in-situ instruments, next to the satellite overpass measurements.

Title Page

Abstract

Introduction

Conclusions

References

Tables

Figures

◀

▶

◀

▶

Back

Close

Full Screen / Esc

Printer-friendly Version

Interactive Discussion



A multi-site IWV techniques intercomparison

R. Van Malderen et al.

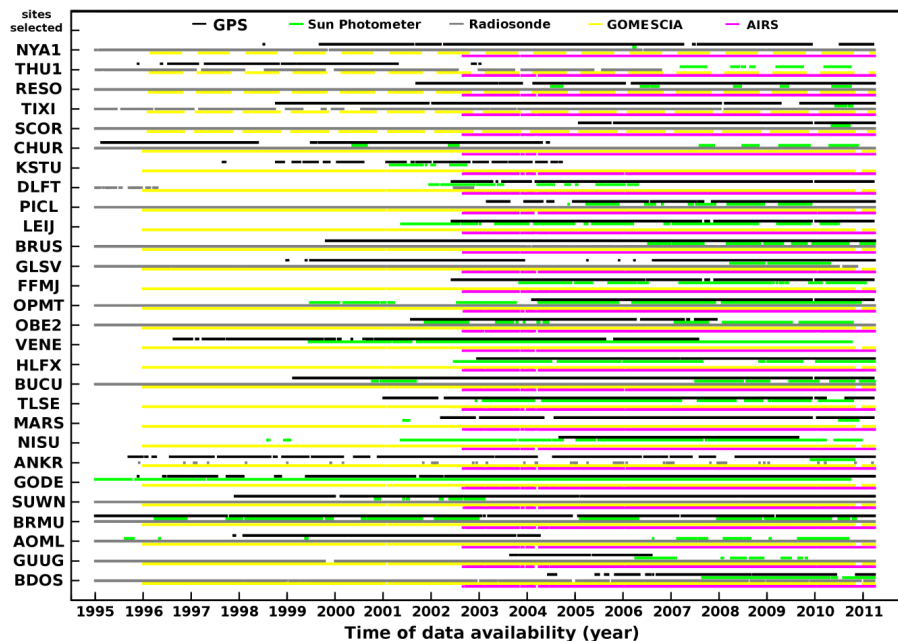


Fig. 3. IWV data availability over the last 15+ yr for the different instruments at the selected sites. Note that, for high latitudes, no GOMESCIA observations are available in winter due to high SZA.

Title Page

Abstract

Introduction

Conclusions

References

Tables

Figures



Back

Close

Full Screen / Esc

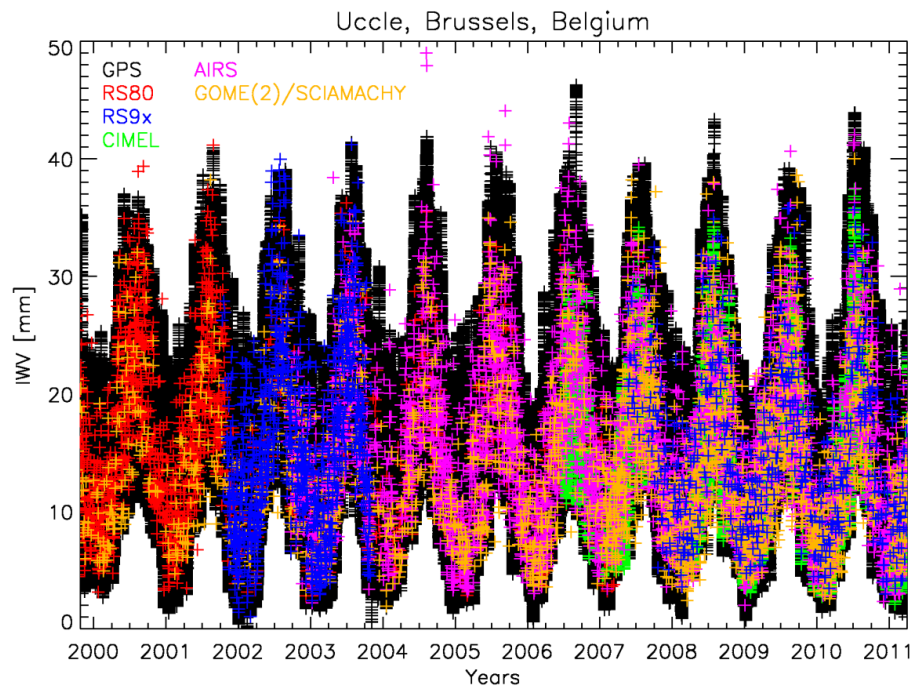
Printer-friendly Version

Interactive Discussion



**A multi-site IWV techniques
intercomparison**

R. Van Malderen et al.

**Fig. 4.** Overview of all IWV data available at Uccle, Brussels, Belgium.

Title Page

Abstract

Introduction

Conclusions

References

Tables

Figures

◀

▶

◀

▶

Back

Close

Full Screen / Esc

Printer-friendly Version

Interactive Discussion



**A multi-site IWV techniques
intercomparison**

R. Van Malderen et al.

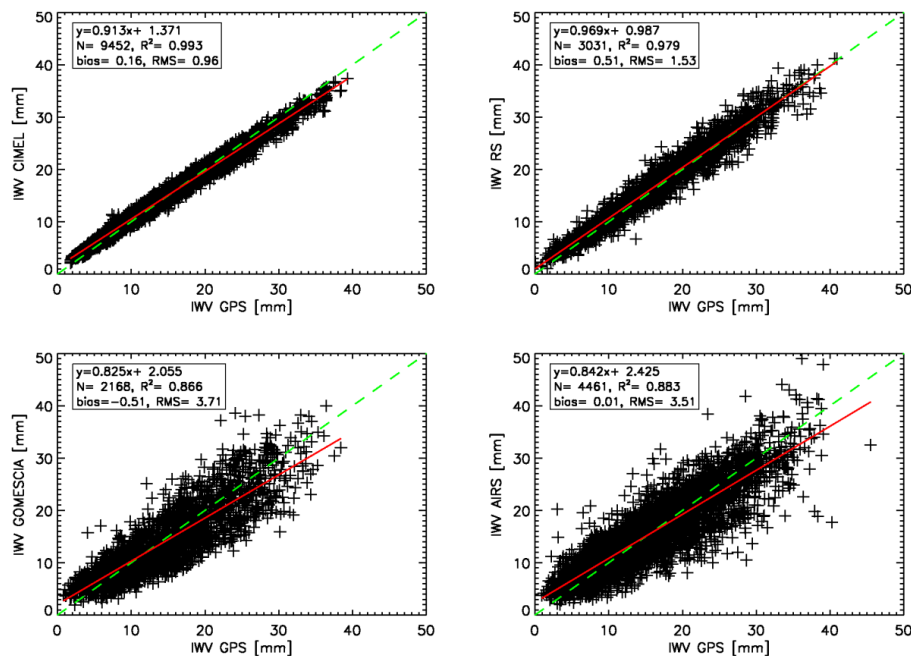


Fig. 5. Scatter plot of coincident IWV measurements of the different instruments with the GPS device at Uccle, Brussels, Belgium.

[Title Page](#)[Abstract](#)[Introduction](#)[Conclusions](#)[References](#)[Tables](#)[Figures](#)[◀](#)[▶](#)[◀](#)[▶](#)[Back](#)[Close](#)[Full Screen / Esc](#)[Printer-friendly Version](#)[Interactive Discussion](#)

A multi-site IWV techniques intercomparison

R. Van Malderen et al.

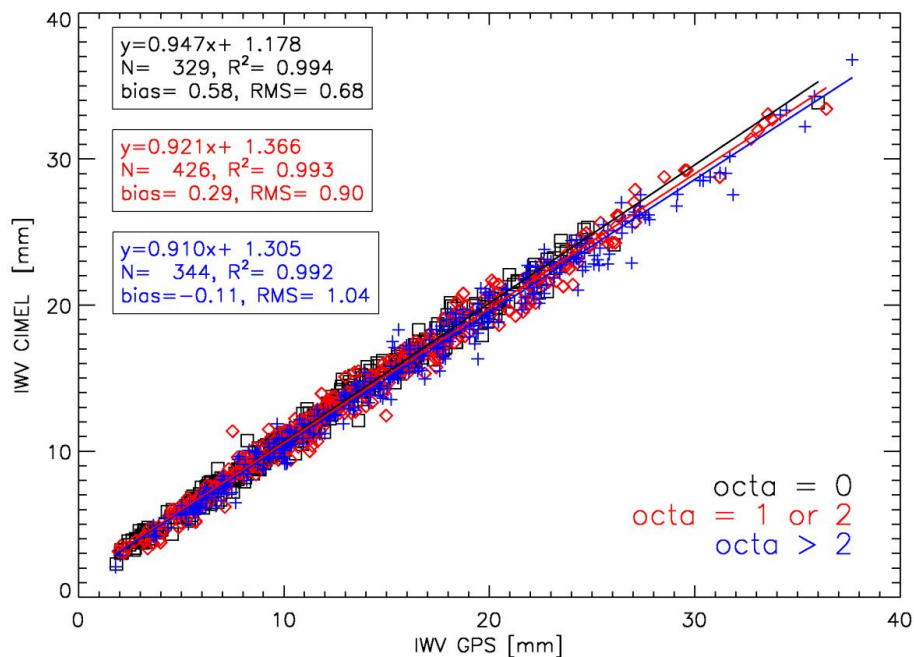


Fig. 6. Scatter plot of coincident IWV measurements of the CIMEL instrument with the GPS device at Uccle, Brussels, Belgium for different classes of cloud cover.

Title Page

Abstract

Introduction

Conclusions

References

Tables

Figures

◀

▶

◀

▶

Back

Close

Full Screen / Esc

Printer-friendly Version

Interactive Discussion



**A multi-site IWV techniques
intercomparison**

R. Van Malderen et al.

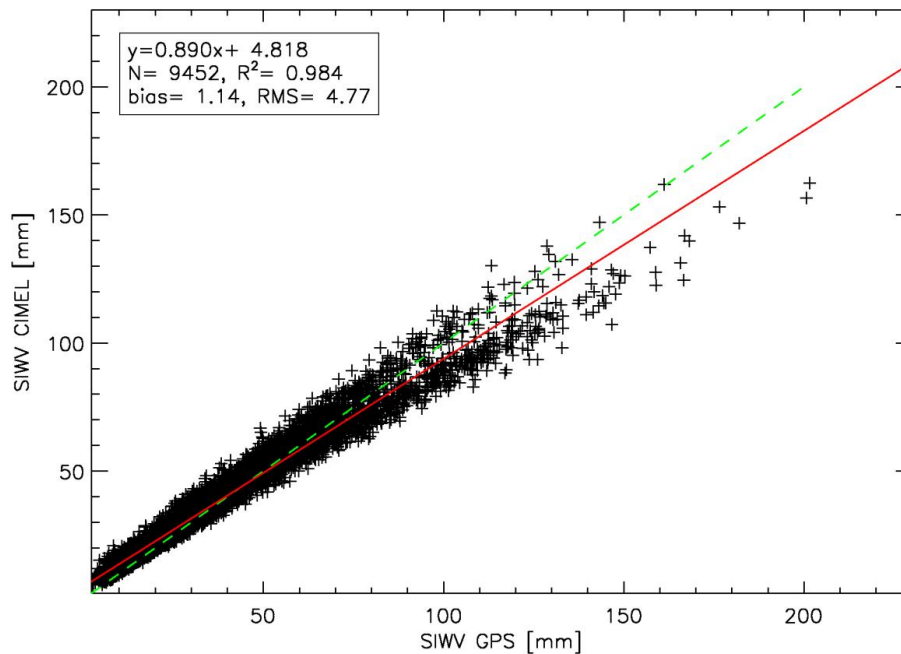


Fig. 7. Scatter plot of coincident solar slant IWV measurements of the CIMEL instrument with the GPS device at Uccle, Brussels, Belgium.

Title Page

Abstract

Introduction

Conclusions

References

Tables

Figures

◀

▶

◀

▶

Back

Close

Full Screen / Esc

Printer-friendly Version

Interactive Discussion



**A multi-site IWV techniques
intercomparison**

R. Van Malderen et al.

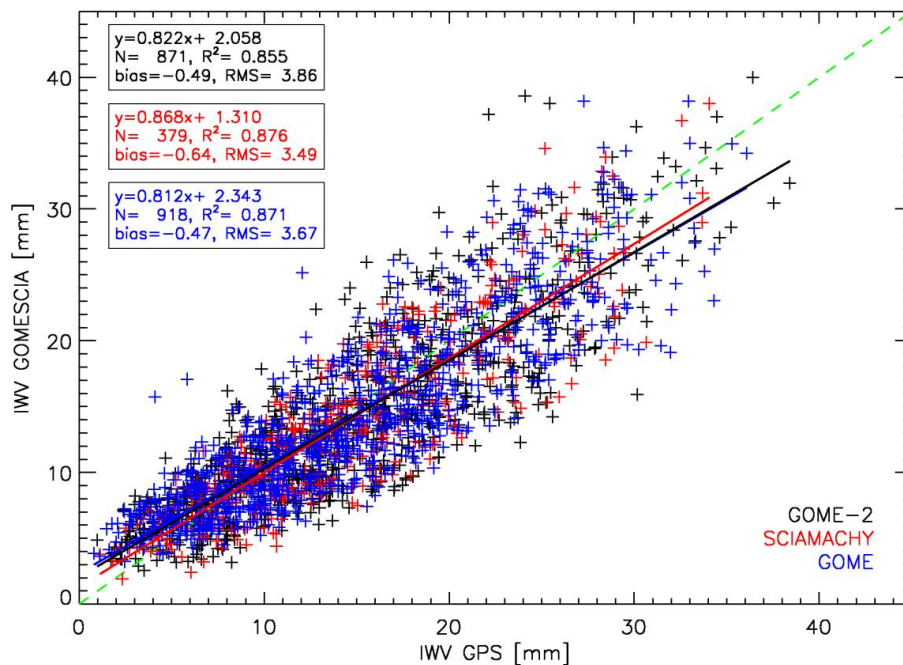


Fig. 8. Scatter plot of coincident IWV measurements of either GOME, SCIAMACHY, or GOME-2 with the GPS device at Uccle, Brussels, Belgium.

Title Page

Abstract

Introduction

Conclusions

References

Tables

Figures

◀

▶

◀

▶

Back

Close

Full Screen / Esc

Printer-friendly Version

Interactive Discussion



A multi-site IWW techniques intercomparison

R. Van Malderen et al.

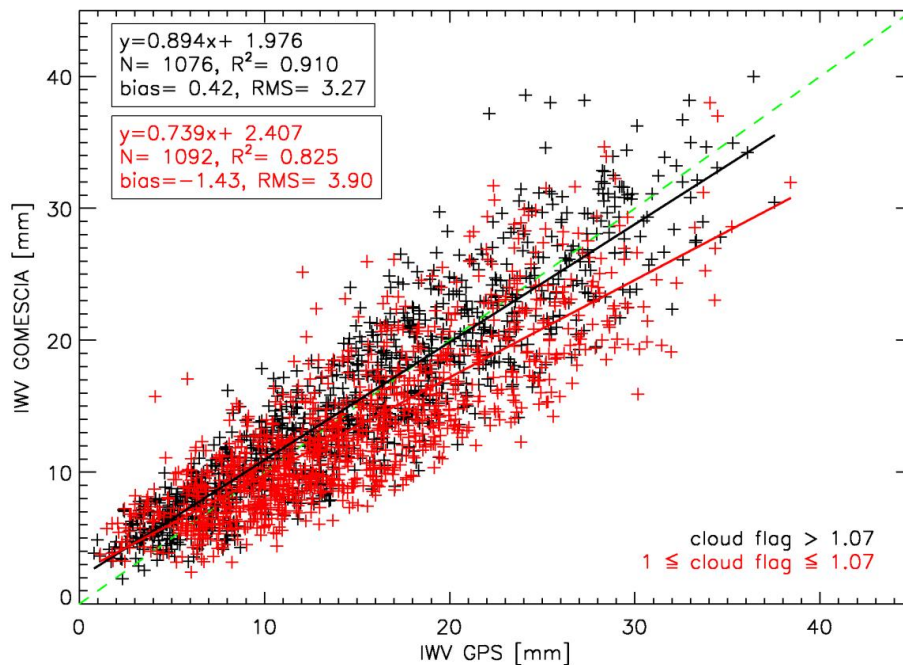


Fig. 9. Scatter plot of coincident IWW measurements of GOMESCIA with the GPS device at Uccle, Brussels, Belgium for two different classes of the GOMESCIA cloud flag.

Title Page

Abstract

Introduction

Conclusions

References

Tables

Figures

◀

▶

◀

▶

Back

Close

Full Screen / Esc

Printer-friendly Version

Interactive Discussion



**A multi-site IWV techniques
intercomparison**

R. Van Malderen et al.

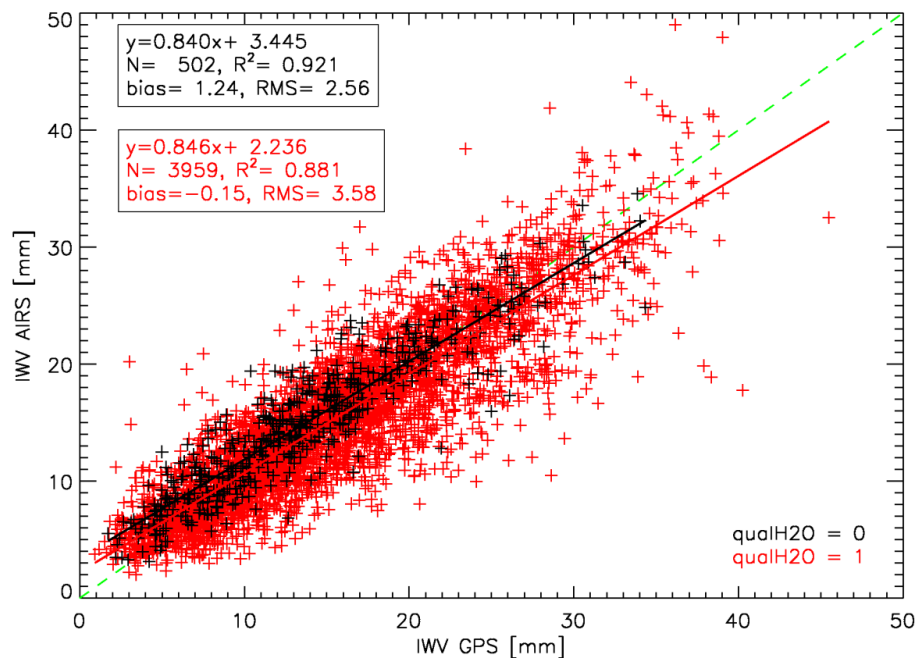


Fig. 10. Scatter plot of coincident IWV measurements of AIRS with the GPS device at Uccle, Brussels, Belgium for the two different quality flags of the AIRS IWV retrievals.

Title Page

Abstract

Introduction

Conclusions

References

Tables

Figures

◀

▶

◀

▶

Back

Close

Full Screen / Esc

Printer-friendly Version

Interactive Discussion



A multi-site IWV techniques intercomparison

R. Van Malderen et al.

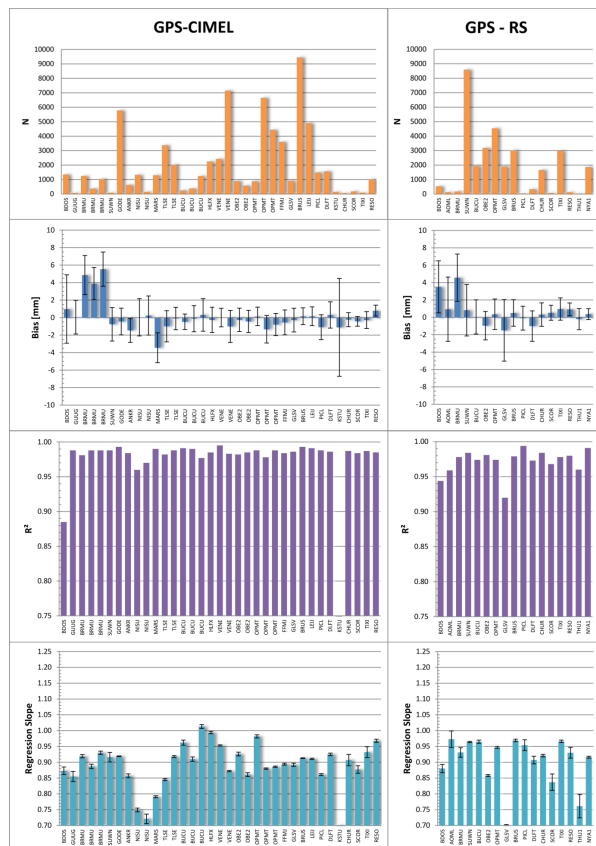


Fig. 11. Column bar plots of scatter plot properties (count N , bias, R^2 and regression slope) of the different CIMEL and radiosonde instruments vs. GPS for the selected sites worldwide. Sites are ordered with increasing latitude. The error bars represent the RMS (bias) and the standard deviation (regression slope).

[Title Page](#)
[Abstract](#)
[Introduction](#)
[Conclusions](#)
[References](#)
[Tables](#)
[Figures](#)

[Back](#)
[Close](#)
[Full Screen / Esc](#)
[Printer-friendly Version](#)
[Interactive Discussion](#)


A multi-site IWV techniques intercomparison

R. Van Malderen et al.

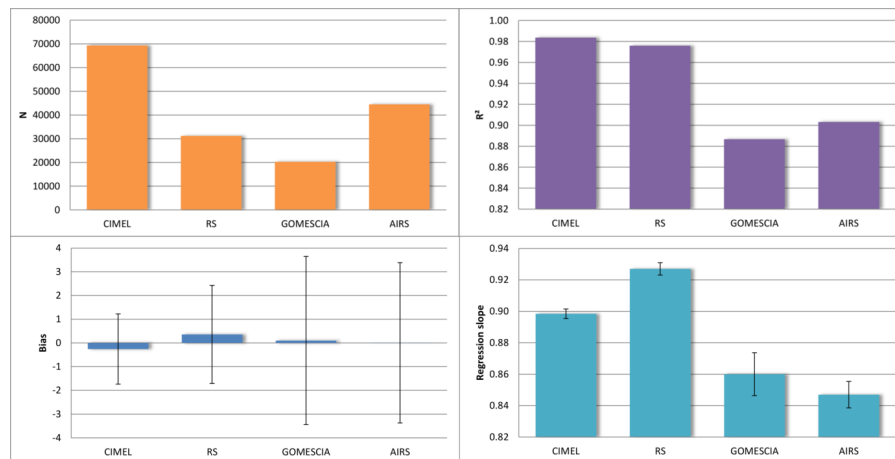


Fig. 13. Column bar plots of scatter plot properties (count N , bias, R^2 and regression slope) of the different instruments vs. GPS averaged over all stations included in the techniques intercomparison. Error bars: see Fig. 12.

Title Page

Abstract

Introduction

Conclusions

References

Tables

Figures

◀

▶

◀

▶

Back

Close

Full Screen / Esc

Printer-friendly Version

Interactive Discussion

